Constructing the Universe with Clusters of Galaxies, IAP 2000 meeting, Paris (France) July 2000
Florence Durret & Daniel Gerbal eds.

RADIAL TEMPERATURE PROFILES OF 11 CLUSTERS OF GALAXIES OBSERVED WITH *BEPPOSAX*

Jimmy A. Irwin and Joel N. Bregman
Department of Astronomy, University of Michigan,
Ann Arbor, MI 48109-1090

We have derived azimuthally-averaged radial temperature profiles of the X-ray gas contained within 11 clusters of galaxies with redshift $z = 0.03 - 0.2$ observed with *BeppoSAX*. Each of the 11 clusters have had their radial temperature profiles previously determined with *ASCA*. We find that the temperature profiles of these clusters are generally flat or increase slightly out to ∼30% of the virial radius, and that a decline in temperature of 14% out to 30% of the virial radius is ruled out at the 99% confidence level. This is in accordance with a previous *ROSAT* PSPC study and an *ASCA* study by White (1999), but in disagreement with an *ASCA* study by Markevitch et al. (1998) that found on average that cluster temperature profiles decreased significantly with radius.

1 Introduction

Knowledge of the radial temperature profile of the hot gas contained within galaxy clusters is a crucial element in determining the total gravitational mass of clusters. Through the equation of hydrostatic equilibrium, the total mass of the cluster can be derived if the density gradient, temperature, and temperature gradient of the gas is known. The latter quantity is the most difficult quantity to obtain, and it has generally been assumed that the gas is isothermal in most previous approaches, since collimated X-ray instruments such as *Ginga* and *EXOSAT* could not determine the temperature structure of clusters.

The assumption of isothermality of the hot gas has been called into question in recent years, mainly as a result of studies done with *ASCA*. The ability of *ASCA* to perform spatially-resolved spectroscopy over the 1–10 keV energy range made it the first X-ray instrument capable of addressing the issue of temperature structure in hot clusters. Many *ASCA* studies have found that the gas within clusters is not isothermal, but decreases with increasing radius, in some cases up to a factor of two (e.g., Markevitch 1996; Markevitch et al. 1998; Markevitch et al. 1999). However, other studies of clusters using *ASCA* data have come to the conclusion that the gas is largely isothermal (e.g., White 1999; Fujita et al. 1996; Ohashi et al. 1997; Kikuchi et al. 1999), at least outside of the cooling radius of cooling flow clusters. A likely cause of this discrepancy is the handling of the large, energy-dependent point spread function (PSF) of *ASCA* that preferentially scatters hard X-rays. This creates an artificial increase in the temperature profile with radius if not dealt with properly. The PSF-correction method applied by Markevitch

et al. consistently leads to significantly decreasing temperature profiles, while other methods (most notably the method of White 1999) lead to isothermal profiles.

The discrepancy among the different PSF-correction methods prompted an analysis of *ROSAT* PSPC data by Irwin, Bregman, & Evrard (1999). Although *ROSAT* was only sensitive to photon energies up to 2.4 keV and was therefore not the most ideal instrument with which to study hot clusters, large (factor of two) differences in temperature should have been detected, but were not. The composite X-ray "color" profiles for 26 clusters in the Irwin et al. (1999) survey indicated isothermality outside of the cooling radius. In fact, a 20% temperature drop within 35% of the virial radius was ruled out at the 99% confidence level.

In this paper, we attempt to resolve the temperature profile discrepancy using *BeppoSAX* data. *BeppoSAX* is sensitive to photon energies up to 10.5 keV, and has a half-power radius that is one-half that of the *ASCA* GIS instrument. In addition, the PSF of *BeppoSAX* is only weakly dependent on energy. Thus, *BeppoSAX* is better-suited for determining temperature profiles for clusters of galaxies than previous X-ray telescopes. Using a sample of 11 clusters found in the *BeppoSAX* archive, we derive radial temperature profiles for each cluster. In a future paper, we will discuss the abundance profiles of the 11 clusters. Throughout this paper, we assume $H_0 = 50$ km s^{-1} Mpc^{-1} and $q_0 = 0.5$.

2 Sample and Data Reduction

From the *BeppoSAX* Science Data Center (SDC) archive (available at http://www.sdc.asi.it/sax_main.html) we have obtained data for seven cooling flow clusters (A85, A496, A1795, A2029, A2142, A2199, and 2A0335+096) and four non-cooling flow clusters (A2163, A2256, A2319, and A3266). All the clusters have redshifts in the range $z = 0.03 - 0.09$ except A2163 ($z = 0.203$). We analyze data from the Medium Energy Concentrator Spectrometer (MECS), which consists of three identical gas scintillation proportional counters (two detectors after 1997 May 9) sensitive in the 1.3–10.5 keV energy range. A detailed description of the MECS is given in Boella et al. (1997). The event files were subjected to the standard screening criteria of the *BeppoSAX* SDC.

Since our goal is spatially-resolved spectroscopy, accounting for scattering from the PSF of the MECS is important. As stated above, scattering from the PSF has an enormous impact on the temperature profiles derived from *ASCA* data. Fortunately, the detector + telescope PSF of *BeppoSAX* is nearly independent of energy, unlike the *ASCA* GIS. This is because the Gaussian PSF of the MECS detector improves with increasing energy, while the PSF of the grazing incidence Mirror Unit degrades with increasing energy (D'Acri, De Grandi, & Molendi 1998), leading to a partial cancellation when these two effects are combined. Still, it is important to account for the PSF accurately when deriving temperature profiles.

To correct for the PSF we have used the routine *effarea*, available as part of the SAXDAS 2.0 suite of *BeppoSAX* data reduction programs. This routine is described in detail in Molendi (1998) and D'Acri et al. (1998). Briefly, *effarea* creates an appropriate effective area file that corrects for vignetting and scattering effects for an azimuthally-symmetric circular or annular region. It does so by creating correction vectors that are a function of energy, and which when multiplied by the observed spectrum yields the corrected spectrum. The surface brightness profile of the cluster (determined from the analysis of *ROSAT* data by Mohr, Mathiesen, & Evrard 1999 and Ettori & Fabian 1999) is convolved with the PSF of the MECS in order to determine the extent to which scattering from other regions of the cluster have contaminated the emission from the extraction region in question. This information is incorporated into the auxiliary response file (the *.arf* file), which is subsequently used in the spectral fitting. The correction to the observed spectrum is modest; D'Acri et al. (1998) and Kaastra, Bleeker, & Mewe (1998) found only small changes between the uncorrected and corrected temperature profiles for Virgo and A2199, respectively. The mismatch in energy bandpasses between the *ROSAT* (0.2–2.4 keV) surface

brightness profile and *BeppoSAX* (1.65–10.5 keV) does not appear to have significantly affected the results.

For each cluster, spectra were extracted from concentric annular regions centered on the peak of emission of the cluster with inner and outer radii of $0'-2'$, $2'-4'$, $4'-6'$, and $6'-9'$. We also extracted one global spectrum from $0'-9'$. At $9'$ the telescope entrance window support structure (the strongback) becomes a factor. In addition, for off-axis angles greater than $10'$, the departure of the PSF from radial symmetry becomes noticeable (Boella et al. 1997). This coupled with the fact that some of the clusters have poor photon statistics outside of $10'$ prompted us to end our profiles at $9'$. At this radius, our temperature profiles extend out to 55% of the virial radius, r_{virial}, for A2163 and 17%–33% for the other clusters, where $r_{virial} = 3.9\ (T/10\ \mathrm{keV})^{1/2}$ Mpc. Background was obtained from the deep blank sky data provided by the SDC. We used the same region filter to extract the background as we did the data, so that both background and data were affected by the detector response in the same manner. The energy channels were rebinned to contain at least 25 counts.

The procedure outlined above does not fit the spectrum of the various regions within the cluster simultaneously. Instead, it assumes a uniform spectrum throughout when correcting for contamination from other regions. Whereas this is not important for the innermost bin (since very few photons are scattered in from larger radii compared to the number of photons truly belonging in the innermost bin), this might affect the outer bins if the temperature profile is varying strongly. This does not seem to be the case though. The spectrum correction vectors presented in D'Acri et al. (1998) for A2199 were quite modest. Other than their innermost bin (which loses some flux via scattering but does not receive much scattered flux from exterior bins), the corrections amounted to 5% or less for energies above 3 keV. In addition, if the exterior bins were significantly contaminated by emission from the interior of the cluster that was at a considerably different temperature, it is likely that no single-component thermal model would give an adequate fit to the data. However, all the spectral fits of the third and fourth spatial bins of the clusters in our study were adequate, with nearly all fits having $\chi_\nu < 1.05$. This coupled with the fact that the PSF-corrected temperatures were not significantly different from the uncorrected temperatures (see § 3.2) indicates that our results are not strongly affected by not fitting the spectra from different regions simultaneously.

For one of the lower temperature clusters (A2199) a long pointed *ROSAT* PSPC observation was available in the HEASARC archive for which no *ROSAT*-determined temperature profile had been published. The observation (RP800644N00) was filtered such that all time intervals with a Master Veto Rate above 170 counts s^{-1} were excluded, in order to discard periods of high background. This resulted in a net exposure of 34,232 seconds. Background was taken from an annulus with inner and outer radii of $30'$ and $40'$. The background was scaled to and subtracted from the source spectra, which were subsequently binned such that each energy channel contained at least 25 counts. Energy channels below 0.2 keV were ignored in the fit.

3 Temperature of the Hot Gas

3.1 Global Temperatures

Using XSPEC we used a MEKAL model with an absorption component fixed at the Galactic value in all spectral fits, except the *ROSAT* PSPC observation of A2199. The temperature, metallicity, and redshift were allowed to vary. Spectral fits of *BeppoSAX* MECS data of the Perseus cluster with the redshift fixed showed significant residuals in the iron line complex region around 6.7 keV (R. Dupke 1999, private communication). These residuals disappeared when the redshift was allowed to vary. The cause of this feature is a systematic shift of 45–50 eV in the MECS channel–to–energy conversion (F. Fiore 1999, private communication). This

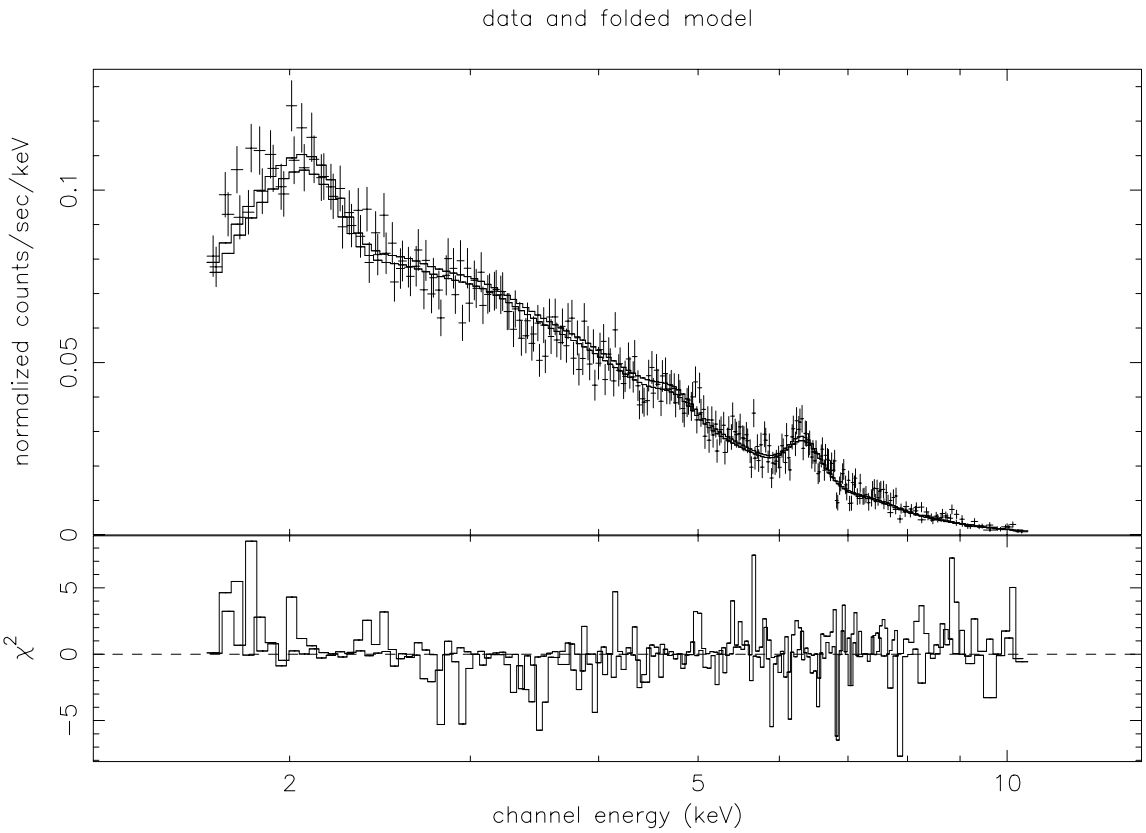

Figure 1: Best-fit MEKAL model spectrum with residuals to the global spectrum of the non-cooling flow cluster A2256 using data in the 1.65–10.5 keV range. An excess of positive residuals below 3.0 keV was a feature common in all 11 clusters analyzed here.

systematic shift was evident in our sample; when the redshift was allowed to vary, the measured redshift was less than the optically-determined redshift in all 11 clusters, and inconsistent with the optically-determined redshift at the 90% confidence level for eight of them. A modest decrease in the reduced χ^2 also occurred for most of the clusters when the redshift was allowed to vary. However, freeing the redshift did not affect the values obtained for the temperature and metallicity significantly (less than a 5% change in either quantity).

With the model described above, we fit the data from MECS2 and MECS3 (and MECS1 when available) separately, but with the same normalization. In accordance with the *Cookbook for BeppoSAX NFI Spectral Analysis* energy channels below 1.65 keV and above 10.5 keV were ignored in the fit. On the whole, the fits to the global spectra were rather poor, ranging from $\chi^2_\nu = 1.13 - 1.8$ for 170–556 degrees of freedom. Inspection of the residuals revealed that the poor fits resulted from excess emission in the 1.65–3.0 keV range. The best-fit spectrum from the non-cooling flow cluster A2256 is shown in Figure 1 and illustrates the positive residuals below 3.0 keV. This effect was even more pronounced in the cooling flow clusters. We performed the fits again, this time only using data in the 3.0–10.5 keV range. The fits were much better, with the fits to all clusters having $\chi^2_\nu \leq 1.20$. In addition, the global temperature values for the fits performed in the 3.0–10.5 keV range were much closer to the global values determined from *ASCA* data (see Table 1). Ten of the 11 temperatures derived from the 1.65–10.5 keV fit were below the *ASCA* value, and in eight cases the 90% error bars did not overlap. Conversely, nine of the 11 temperatures derived from the 3.0–10.5 keV fit have 90% errors bars that overlap with the error bars from the *ASCA* temperatures. All quoted errors are 90% confidence levels unless otherwise noted.

Since the improvement in χ^2_ν when channels in the 1.65–3.0 energy range were excluded was more pronounced for the cooling flow clusters than in the non-cooling flow clusters, we

Table 1:

GLOBAL TEMPERATURE FITS

Cluster	*ASCA*[a]	*BeppoSAX* 1.65–10.5 keV		*BeppoSAX* 3.0–10.5 keV	
	kT (keV)	kT^b (keV)	χ_ν/d.o.f.	kT^b (keV)	χ_ν/d.o.f.
A85	6.1 ± 0.2	$5.6^{+0.1}_{-0.1}$	1.70/340	$6.4^{+0.3}_{-0.2}$	1.17/282
A496	4.3 ± 0.2	$3.7^{+0.1}_{-0.1}$	1.59/317	$4.2^{+0.1}_{-0.1}$	1.20/259
A1795	6.0 ± 0.3	$5.0^{+0.2}_{-0.2}$	1.14/269	$6.0^{+0.4}_{-0.4}$	0.97/211
A2029	8.7 ± 0.3	$6.7^{+0.2}_{-0.2}$	1.26/170	$7.6^{+0.5}_{-0.4}$	0.98/141
A2142	8.8 ± 0.6	$7.6^{+0.2}_{-0.2}$	1.32/350	$8.7^{+0.4}_{-0.4}$	1.02/292
A2163	11.5	$11.0^{+0.6}_{-0.6}$	1.32/556	$11.7^{+1.0}_{-0.9}$	1.05/440
A2199	4.4 ± 0.2	$4.0^{+0.1}_{-0.1}$	1.58/506	$4.4^{+0.1}_{-0.1}$	1.03/419
A2256	7.5 ± 0.4	$6.2^{+0.3}_{-0.3}$	1.13/296	$7.1^{+0.5}_{-0.4}$	1.06/238
A2319	9.2 ± 0.7	$8.8^{+0.3}_{-0.4}$	1.27/331	$10.5^{+0.8}_{-0.7}$	1.04/273
A3266	7.7 ± 0.8	$8.0^{+0.4}_{-0.3}$	1.15/323	$9.9^{+0.8}_{-0.7}$	0.93/265
2A0335+096	~ 3.4[c]	$2.80^{+0.03}_{-0.04}$	1.80/315	$3.20^{+0.08}_{-0.08}$	1.13/257

[a] Single-fit temperature from Markevitch et al. (1998).

[b] Errors listed are 90% confidence levels.

[c] Estimated value inside of $10'$ from radial temperature profile of Kikuchi et al. (1999).

investigated the possibility that the excess emission below 3.0 keV was a result of a cooling flow component. Indeed, the addition of a cooling flow model to the MEKAL model provided a substantially better fit in the 1.65–10.5 keV case, and in some cases the fit became formally acceptable. However, the inferred cooling rates were several hundred solar masses per year higher than previous published values (e.g., Peres et al. 1998). In fact, cooling rates of several hundred solar masses per year were found for the non-cooling flow clusters A2163, A2256, A2319, and A3266. In addition, cluster far from the cluster center, where no cooling gas should be found. This clear contradiction illustrates how a physically implausible model can still yield good spectral fits, and the danger in interpreting such a result. We conclude that although some of the excess emission in the 1.65–3.0 keV range is from cooling gas, there is a clear excess of soft emission beyond what is expected from cooling gas, possibly due to uncertainties in the calibration of the MECS instruments. Since including this energy range leads to global temperatures significantly below the *ASCA* value, we only fit the data in the 3.0–10.5 keV range for the remainder of the paper. Given the good agreement in the 3.0–10.5 keV fit and the ASCA-determined temperatures, we are confident of the calibration of *BeppoSAX* above 3.0 keV.

3.2 Radial Temperature Profiles

The PSF-corrected and -uncorrected radial temperature profiles for each of the 11 clusters are shown in the left panels of Figure 2. As was found in previous studies, correction for the MECS PSF does not seriously affect the temperature profile. In the right panels are our *BeppoSAX* temperature profiles along with temperature profiles derived from other *ASCA* and *BeppoSAX* studies for comparison. We note that for A85, A496, A1795, A2029, A2142, and A2199 the innermost bin has been fit with a cooling flow component in addition to a thermal model for the profiles of Markevitch et al. (1998), Markevitch et al. (1999), and Sarazin, Wise, & Markevitch (1998), which accounts for the large discrepancy in this bin compared to other studies that fit the spectra with only single-component models.

A85: We have included the subclump to the south of the cluster center in our analysis. Outside of the cooling radius, the temperature profile increases moderately from 6.4 keV to 7.9 keV at a significance level of 2.2σ. This is in agreement with the *ASCA* analysis by White (1999), but contrasts with Markevitch et al. (1998) who found a profile that decreased from 8.0 keV in a $1.5' - 6'$ annular bin to 6.3 keV in a $6' - 12'$ annular bin with *ASCA* data. Pislar et al. (1997) and Kneer et al. (1995) analyzed *ROSAT* PSPC data for this cluster and found a roughly isothermal profile outside the cooling region. However, the *ROSAT* analysis found a significantly lower temperature, with most of the cluster below 5 keV. This is possibly due to a gain calibration problem of the *ROSAT* PSPC instrument.

A496: This nearby cluster ($z = 0.0326$) has a cooling rate of $\dot{M} = 95\ M_{\odot}\ \mathrm{yr}^{-1}$ (Peres et al. 1998). The temperature is lowest in the center (typical of a cooling flow), and is consistent with a constant value of 4.5–5.0 keV at larger radii. This is consistent with the *ASCA* analysis of Dupke & White (1999), who did not perform a PSF correction. For low temperature clusters, the PSF does not introduce a significant spurious positive gradient to the temperature profile (Takahashi et al. 1995). The profile of White (1999) also agreed for the most part with our profile, although one of their bins deviated by $\sim 2\sigma$ from ours. Markevitch et al. (1999) found a continuous drop in temperature of 5.6 keV to 3.5 keV from a $2' - 5'$ annular bin to a $10' - 17'$ annular bin.

A1795: We find a temperature profile consistent with a temperature of 6–7 keV outside of the cooling flow region. A significant decrease in temperature was not found in the center for this cooling flow cluster. This result is similar to the *ASCA* results of Mushotzky et al. (1995; uncorrected for the PSF), White (1999), and Ohashi et al. (1997), although the Ohashi et al. (1997) result found a somewhat lower overall temperature for this cluster. Markevitch et al. (1998) detected a decline in temperature with radius, but not at a high significance with *ASCA*. *ROSAT* found a low temperature in the inner cooling flow region, and a moderately increasing profile at larger radii (Briel & Henry 1996). The discrepancy in the innermost bin is likely the result of the low energy bandpass (0.1–2.4 keV) of *ROSAT* sampling lower temperature gas than the higher energy bandpass (3.0–10.5 keV) of *BeppoSAX* in the cooling region.

A2029: We find a basically flat temperature profile out to $6'$ and a marginally significant (1.7σ) rise from $6' - 9'$, consistent with the *ASCA* analysis of White (1999). This is the opposite trend found by Sarazin et al. (1998) with *ASCA* data, who found a decline in temperature from $\sim$9 keV to 6 keV outside of $5'$ (but with large errors in the outer regions). Still, they found that an isothermal profile was rejected at the $> 96\%$ confidence level. This was one of the few clusters for which Irwin et al. (1999) found evidence for a statistically significant temperature decline with *ROSAT* data, although the drop did not occur until outside of $10'$. Molendi & De Grandi (1999) analyzed the same *BeppoSAX* data and found a temperature profile consistent with 8 keV out to $8'$ and dropping to 5 keV from $8' - 12'$ (see § 4.3 for a detailed comparison of the two analyses).

A2142: We find a very flat profile with a temperature of 8–9 keV. A similar result was found by White (1999), although the errors were large. Markevitch et al. (1998) found evidence for a temperature decline, but not at a high significance level. Henry & Briel (1996) analyzed *ROSAT* data and found temperatures of 10 keV or higher outside the cooling region, with a peak in the $2.5' - 5'$ bin.

A2163: This cluster has the highest redshift in our sample ($z = 0.203$), and is also the hottest. The cluster does not possess a cooling flow and probably underwent a merger in the recent past (e.g., Elbaz, Arnaud, & Böhringer 1995). Since the centroid of the cluster lies over $5'$ from the detector center, we have excluded data from behind the strongback support structure and beyond. We have included data in the last annular bin out to $12'$ (as long as it fell inside the strongback) to improve the statistics in the last bin. Our profile extends out to 73% of the virial radius, considerably farther than any other cluster in our sample. We find that the

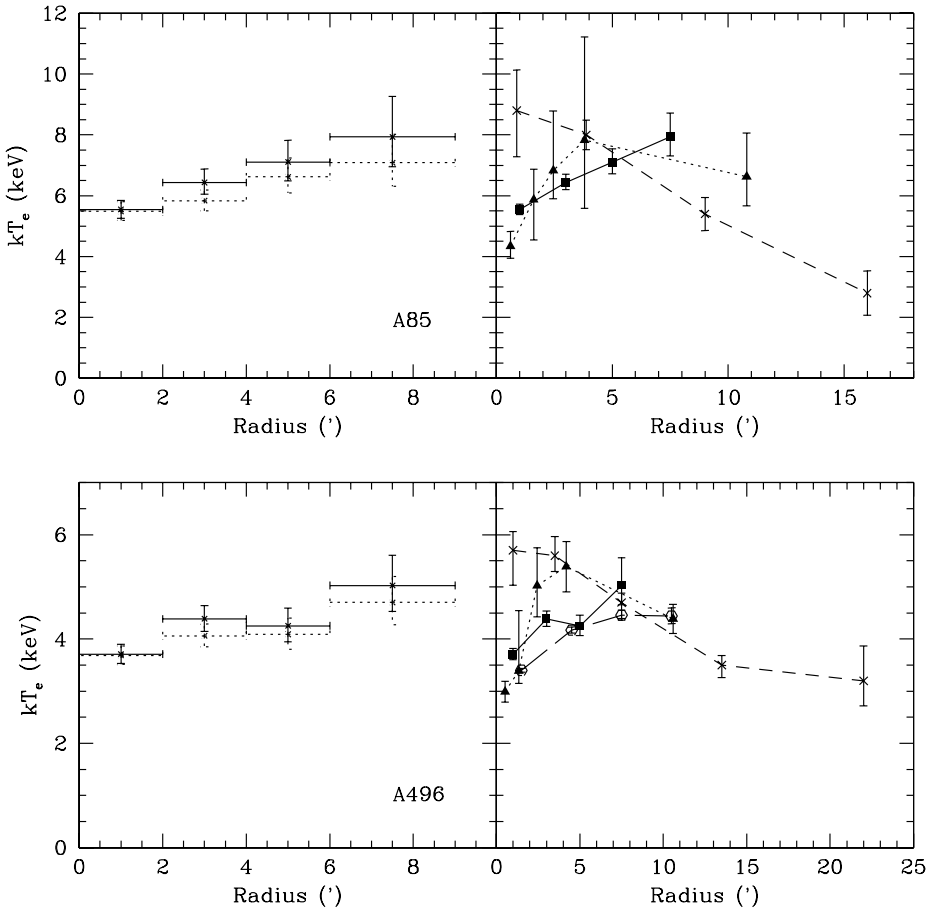

Figure 2: Radial temperature profiles for the 11 clusters in the sample, derived from fitting in the 3.0–10.5 keV range. In the left panel, solid lines represent temperatures corrected for the PSF of *BeppoSAX* and the dotted lines are not corrected. Error bars are 90% confidence levels. The right panels compare our results (filled squares and solid lines) with temperature profiles derived from *ASCA* data using the method of White (1999; filled triangles and dotted line), the method of Markevitch et al. (1996; crosses and dashed lines), uncorrected *ASCA* profiles from Dupke & White (1999) and Kikuchi et al. (1999) (open hexagons and long dashed line in A496 and 2A0335+096), and *BeppoSAX* profiles for A2029, A2199, A2319, and A3266 (open triangles and long dashed lines). For the right panels, the error bars are 1σ confidence levels.

cluster has a temperature of 10–11 keV out to $4'$, before experiencing a marginally significant ($< 2\sigma$) rise in temperature at larger radii. The errors are quite large at large radii, although the temperature is greater than 8 keV at the 90% level. This agrees with the *ASCA* result of White (1999), but disagrees strongly with the result from *ASCA* and *ROSAT* by Markevitch et al. (1996), who found temperatures of $12.2^{+1.9}_{-1.2}$, $11.5^{+2.7}_{-2.9}$, and $3.8^{+1.1}_{-0.9}$ for annular bins of $0' - 3'$, $3' - 6'$, and $6' - 10'$ in extent, respectively. For these regions, we find temperatures of $10.1^{+0.9}_{-0.8}$, $11.7^{+2.6}_{-1.8}$, and $13.2^{+17.9}_{-4.6}$, respectively, using only data inside the strongback (90% errors). Thus, the outermost bin of the *BeppoSAX* data differs from that of Markevitch et al. (1998) at the 3.3σ confidence level.

A2199: Outside of the cooling flow region, we find a constant temperature of about 4.5 keV. Analysis of the same *BeppoSAX* data by Kaastra et al. (1998) and of *ASCA* data by White (1999) found a similar result. However, Markevitch et al. (1999) found a steadily decreasing profile from 5.2 keV to under 5 keV at $7.5'$, with a further decline at larger radii with the same *ASCA* data.

We have analyzed the *ROSAT* PSPC data for this cluster, and derived a temperature profile out to $18'$ (0.9 Mpc). The angular extent of this cluster is large, so to confirm that our

background region was not significantly contaminated by the cluster emission, we derived a temperature

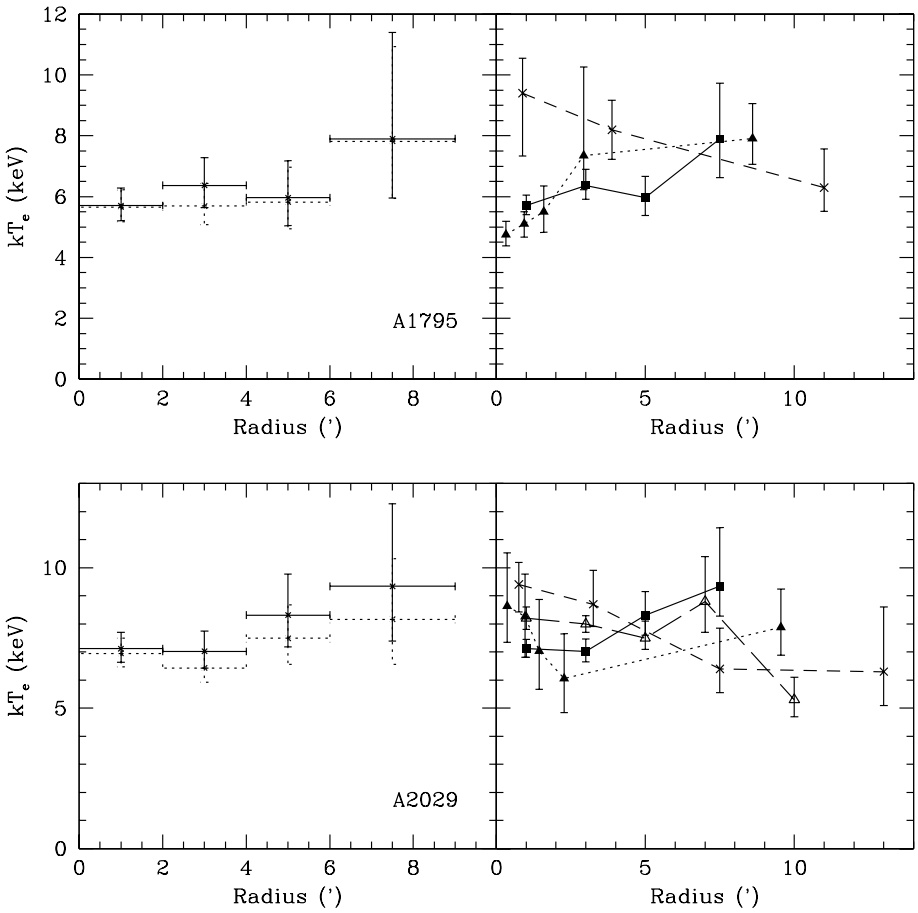

Fig. 2 – continued.

profile using a background annulus of $40' - 50'$ and found the same results as we did with a background annulus of $30' - 40'$. The temperature profile is shown in Figure 3. The profile shows a drop in the center indicative of a cooling flow. At large radii the profile is flat. However, the *ROSAT*-derived temperature is significantly lower than the value from *ASCA* or *BeppoSAX*. Whereas this might be expected in the central cooling flow region where *ROSAT* is sampling cooler gas than the other instruments because of its low energy bandpass, this tendency persists outside the cooling region. From $2' - 9'$, the temperature is 3.2 ± 0.2 keV, whereas it is 4.5 ± 0.1 for *BeppoSAX*. Data from *ROSAT* appears sometimes to have a tendency to measure lower temperatures than other instruments for clusters, such as A3558 (Markevitch & Viklinin 1997) and A85 (see above).

To compensate for this effect, we have adjusted the gain of the observation such that the temperature in the $2' - 9'$ region matched that of *BeppoSAX*. We excluded the inner $2'$ to avoid complications from the cooling flow region. An adjustment of 1.5% in the gain was necessary to bring the global temperature determined by the two instruments into agreement. A gain adjustment of this magnitude was within the range of values found by Henry & Briel (1996) when they analyzed five different pointings of A2142 with *ROSAT*. With this new gain value the temperature profile remains flat outside of the cooling region out to $18'$ (35% of the virial radius), albeit at a higher value than before. The main conclusion drawn from the *ROSAT* result of A2199 is that the temperature profile appears flat outside of the cooling flow region regardless of whether or not the gain was adjusted.

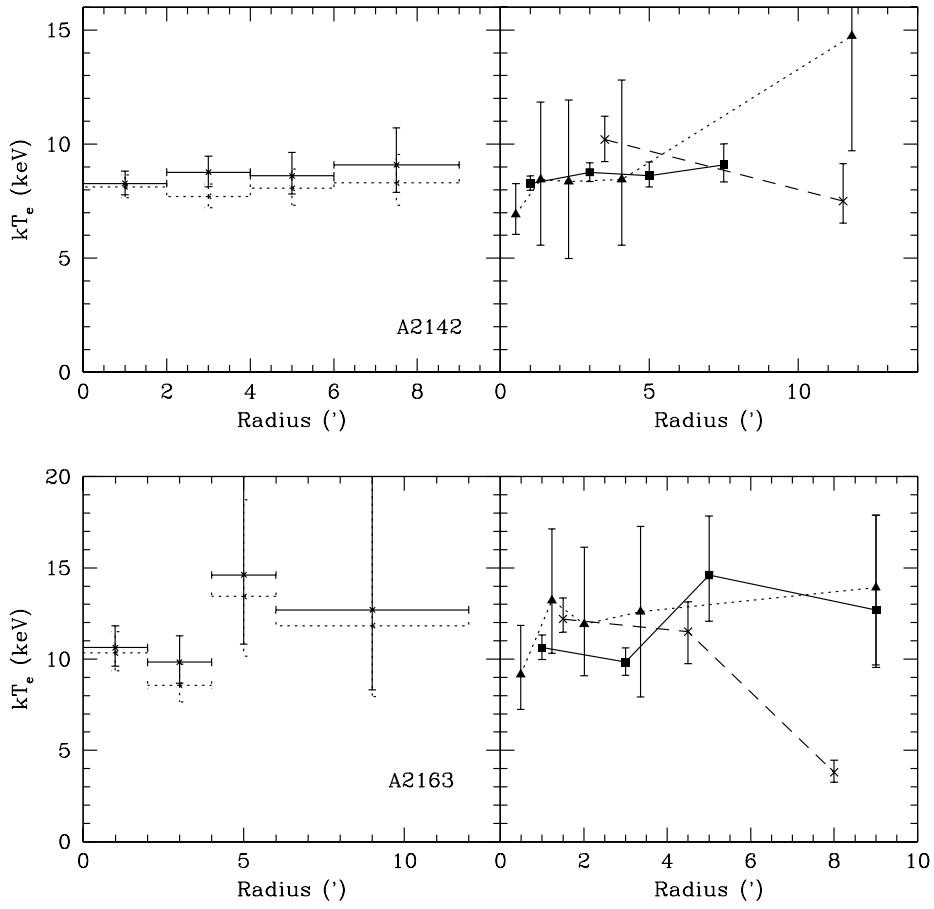

Fig. 2 – continued.

A2256: We find a flat temperature profile consistent with a temperature of 7 keV, in excellent agreement with the *ASCA*-determined profile of White (1999). This contrasts with the Markevitch (1996) result from *ASCA* which found the temperature to decrease from 8.7 keV to 7.3 keV from the $0' - 6'$ to $6' - 11'$, with a steep drop to 4 keV at larger radii. Markevitch (1996) claims that the *ROSAT* data confirm this result, albeit with larger errors, contrary to the claim of Briel, & Henry (1993) who analyzed the same *ROSAT* data and found a roughly isothermal profile.

A2319: We find a flat temperature profile out to $6'$ and a marginally significant ($\sim 2\sigma$) increase from $6' - 9'$. This is consistent with the White (1999) result. Markevitch (1996) also found an isothermal profile out to $10'$ with *ASCA*, and a decreasing profile at larger radii. The *ROSAT* data suggested isothermality (Irwin et al. 1999). Molendi et al. 1999 analyzed the same *BeppoSAX* data and found a flat temperature profile out to $16'$.

A3266: This probable merging cluster exhibits a slight increase in temperature in the center and levels off at radii out to $9'$. With *ASCA* data, Markevitch et al. (1998) found a steady decrease in temperature from almost 10 keV in the central $2.5'$ to 5 keV outside of $10'$, and White (1999) also found a modestly decreasing profile (from 9 keV to 7.5 keV). The *ROSAT* data suggested isothermality although a modest decrease in temperature could not be ruled out (Irwin et al. 1999). De Grandi & Molendi (1999) analyzed the same *BeppoSAX* data and found a more substantial decrease in temperature, with a drop from 10 keV in the center to 4.5 keV out to $20'$.

2A0335+096: The coolest cluster in our sample, 2A0335+096 possesses a rather strong cooling flow (400 $M_\odot$ yr^{-1}; Irwin & Sarazin 1995). The temperature is lowest in the innermost

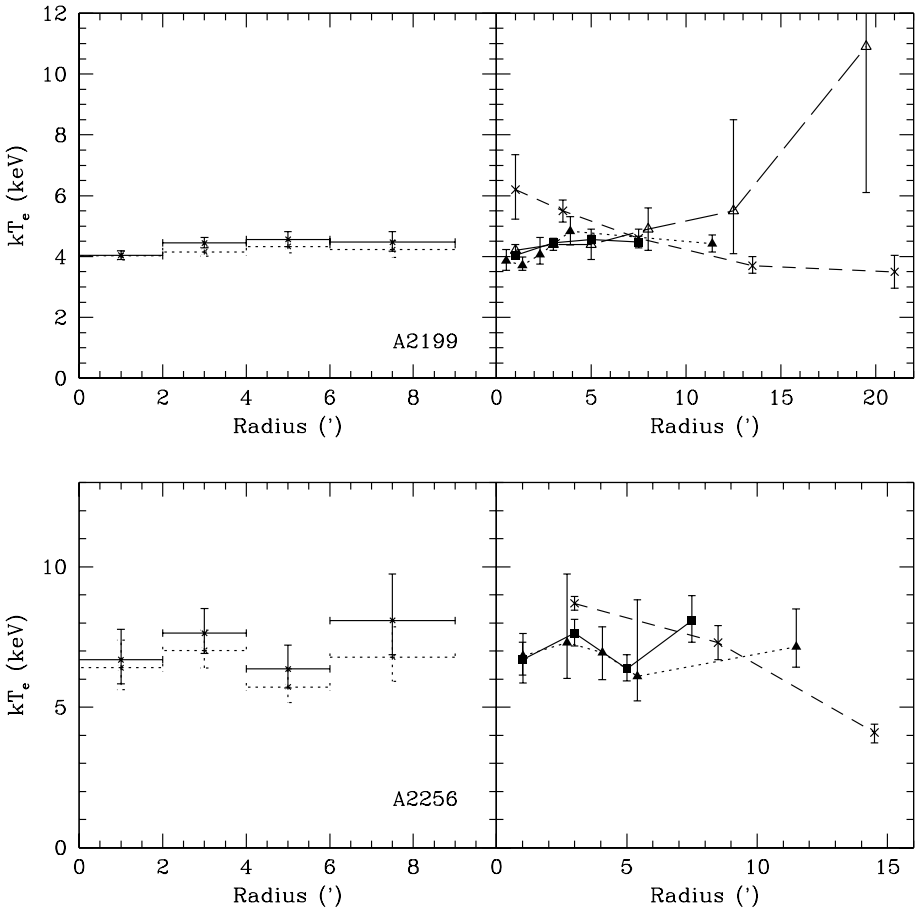

Fig. 2 – continued.

bin and levels off to a value of 3.4 keV out to 9′. Kikuchi et al. (1999) analyzed the *ASCA* data for this cluster and found a flat temperature profile out to 10′, while White (1999) found a flat profile out to 4′ and a jump to 4.6 keV at larger radii.

In conclusion, the temperature profiles of the 11 clusters in our sample are roughly constant, and in general agreement with those derived from *ASCA* data by White (1999). This is in in disagreement with the profiles derived from the same *ASCA* data with the method of Markevitch et al. (1996), which find a significant decrease in temperature in many of the clusters. A more detailed comparison is given in § 4.

3.3 Normalized Temperature Profiles

In Figure 4*a* we plot the temperature profiles normalized to the global temperature for all 11 clusters versus radius in units of the virial radius, r_{virial}. The error bars represent the 1 σ uncertainties. At small radii, the normalized profiles are typically less than one, owing to the presence of cooling flows in seven of the 11 clusters. As a result of the low temperature in the center, the outer regions are necessarily normalized to a value greater than one. To compensate for this effect, we have calculated global temperatures for the seven cooling flow clusters excluding the inner 2′, and then normalized the $2' - 4'$, $4' - 6'$, and $6' - 9'$ bins by this temperature, while excluding the innermost bin. The result is shown in Figure 4*b*. Out to 20% of the virial radius, the temperature profiles appear flat. From 20% to 30% of the virial radius, the profiles rise somewhat, although the temperatures are not well constrained in this region. Most of the values are consistent with unity at the 1σ confidence level.

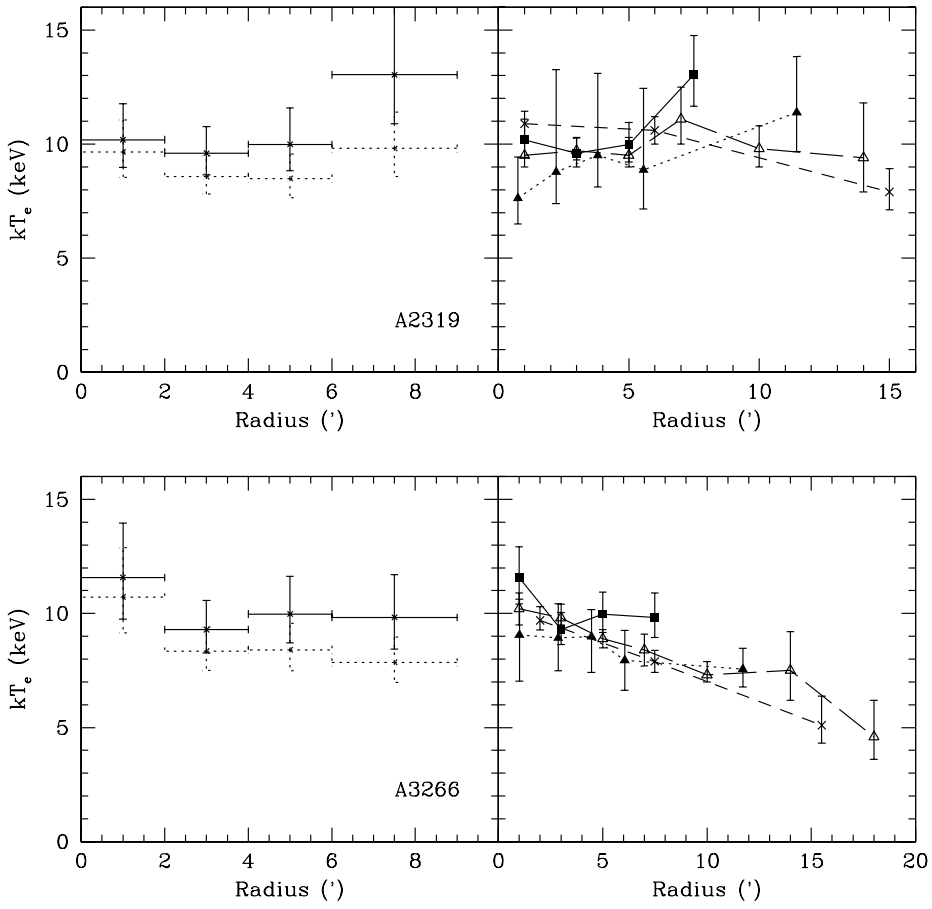

Fig. 2 – continued.

A constant temperature model ($T/T_{mean} = 1$) provided a good fit to the data ($\chi^2 = 43.7$ for 37 degrees of freedom). A linear model of the form $(T/T_{mean}) = a + b(r/r_{virial})$ provided a somewhat better fit ($\chi^2 = 36.0$ for 35 degrees of freedom), with values of $a = 0.942$ and $b = 0.440$. The 90% confidence range on the slope b was 0.123–0.752. This best-fit line is shown in Figure 4*b*, with the dashed lines representing the 90% confidence levels on the slope of the line. We find that a temperature drop of 14% from the center out to 30% of the virial radius can be ruled out at the 99% confidence level.

The data indicate that the gas is isothermal or mildly increasing in temperature out to 30% of the virial radius ($1.0h_{50}^{-1}$ Mpc for a 7 keV cluster). Beyond this radius, the temperature profile may well decline. Most hydrodynamical cluster simulations predict a drop in temperature past 50% of the virial radius (see, e.g., Frenk et al. 1999). *XMM* will be the ideal instrument for determining the temperature profiles of clusters at large radii.

4 Comparison to Other Results

The presence of temperature gradients in clusters of galaxies has been a topic of hot debate in recent years, and there have been many investigations as to the temperature structure of clusters. Here, we summarize previous results grouped by X-ray telescope and compare them to our results.

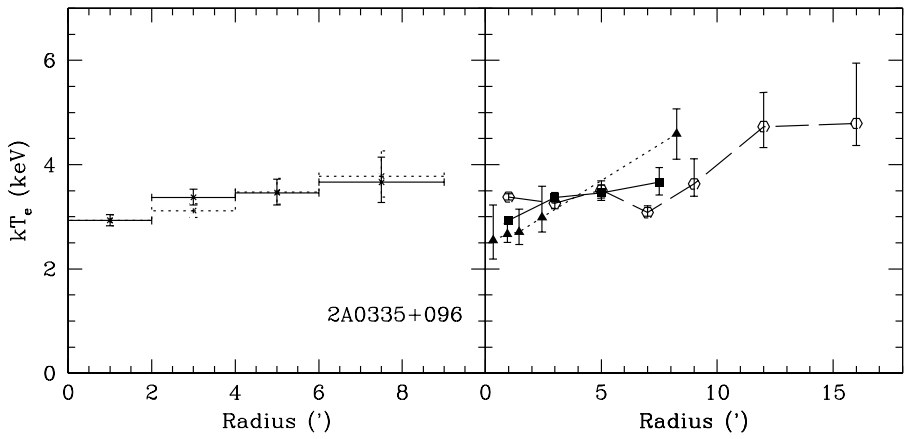

Fig. 2 – continued.

4.1 Temperature Profiles Determined With ASCA

The claim of the existence of large temperature declines with radius was first suggested following the results from *ASCA* data using the PSF-correction technique of Markevitch et al. (1996), including Markevitch (1996), Markevitch et al. (1998), Sarazin et al. (1998), and Markevitch et al. (1999). Markevitch et al. (1998) observed 30 clusters with *ASCA* and found in general that the temperature profiles declined with radius (up to a factor of two), and that the decline was described well by a polytropic equation of state, i.e.,

$$T(r) \propto \left(1 + \frac{r^2}{a_x^2}\right)^{-3\beta(\gamma-1)/2}, \qquad (1)$$

where r is the projected distance, a_x is the core radius, β has its usual meaning in the context of isothermal β-models, and γ is the polytropic index. The best-fit polytropic index was $\gamma = 1.24^{+0.20}_{-0.12}$ (90% confidence levels). This model clearly does not fit the *BeppoSAX* data. The polytropic fit led to $\chi^2 = 577$ for 37 degrees of freedom.

It was pointed out by Irwin et al. (1999) that the trend in the temperature profile found by the method of Markevitch et al. (1996) differed from that found by other PSF-correction techniques from various authors (e.g., Ikebe 1995; Fujita et al. 1996; Kikuchi et al. 1999). Of the 28 clusters analyzed using the method of Markevitch et al. (1996) that did not show very strong evidence for a merger, 22 (14) of them were inconsistent with a constant temperature profile at the 70% (90%) probability level. Conversely, clusters analyzed using the method of Ikebe (1995), Fujita et al. (1996), or Kikuchi et al. (1999) were found to have basically flat temperature profiles, with all 11 clusters consistent with a constant temperature.

Of particular interest are clusters analyzed by more than one method, or clusters whose temperature is low enough that the PSF of *ASCA* does not influence the temperature profile significantly (for clusters below 5 keV). A399, A401, MKW3S, A1795, and A496 are examples where the method of Markevitch et al. (1996) leads to different trends in the radial temperature profiles than with other methods (Fujita et al. 1996; Kikuchi et al. 1996; Ohashi et al. 1997; Dupke & White 1999). The latter two are also in our sample, and show no evidence for a decline in temperature outside of the cooling region (Figure 2).

Recently, White (1999) has determined the temperature profiles of a large number of clusters observed with *ASCA* using the PSF-correction technique outlined in White & Buote (1999). He found that 90% of the 98 clusters in his sample were consistent with isothermality at the 3σ

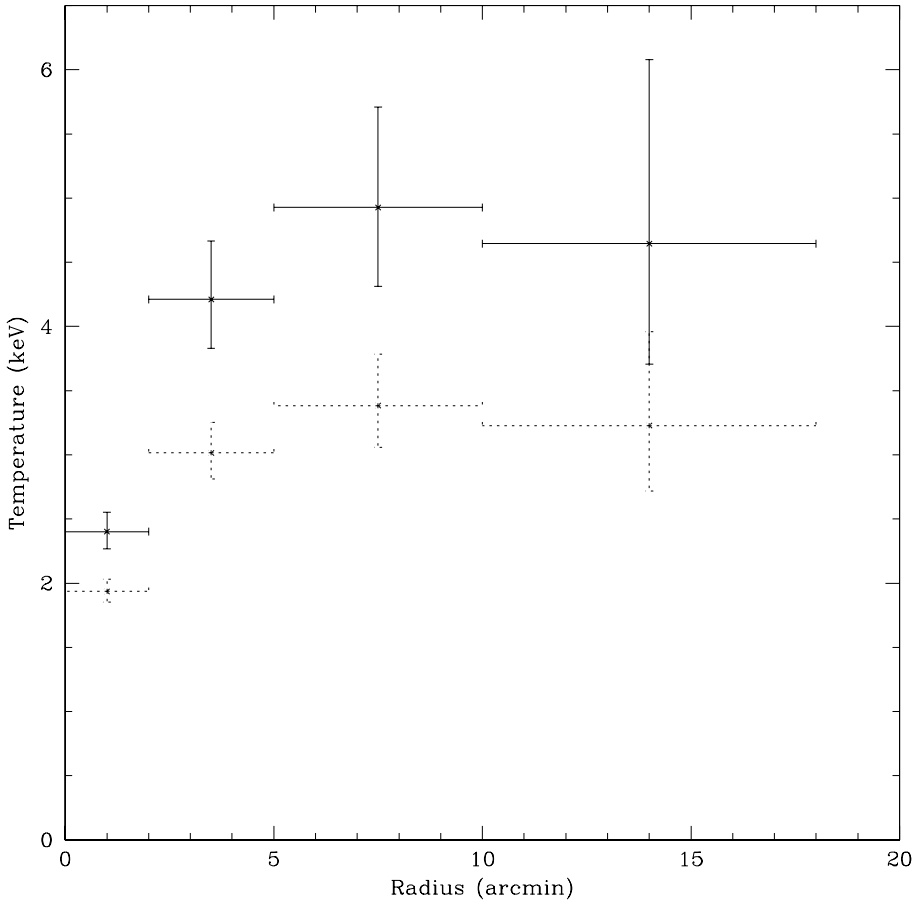

Figure 3: Temperature profile of A2199 derived from the *ROSAT* PSPC with 90% error bars. Outside of the cooling radius, the temperature profile is flat both in the case where the gain is set to the nominal value (dotted line) or adjusted such that the temperature in the $2' - 9'$ region is normalized to the temperature derived from *BeppoSAX* for the same region (solid line).

confidence level. On a cluster by cluster comparison of the 11 clusters common in both samples, we find our temperature profiles are in excellent agreement with those of White (1999), with only two exceptions. Our temperature value of the outermost bin of A3266 is $\sim$2 keV higher than the value of White (1999). However, the 1σ error bars just touch so this discrepancy is not at a high significance. Also, our temperature profile of A496 differs somewhat from his. This difference occurs around $4'$ and is significant at $\sim 2\sigma$. However, given that we have 44 temperature values for the 11 clusters, it is not unreasonable that two of our values differ by 2σ. In fact, this is the number of 2σ discrepancies one would expect from a statistical point of view.

Given the conflicting results regarding this topic, it is worthwhile to examine the PSF-correction techniques of the two largest studies, namely those using the techniques of Markevitch et al. (1996; hereafter method M) and White & Buote (1999; hereafter method WB). Both techniques assume a spatial distribution for the cluster emission; method M assumes the emissivity profile obtained from *ROSAT* PSPC data for the cluster in question, while method WB assumes the spatial distribution derived from a maximum-likelihood deconvolution of the *ASCA* image. Method M creates simulated events drawn from this spatial distribution and from an initial guess for the cluster spectrum, and convolves the events with the spatially-variable PSF. The input cluster spectrum is varied until the simulated data matches the actual data. Method WB ray-traces events drawn from the spatial distribution through the telescope optics and attempts to find the most likely association between events in the deconvolved and convolved planes on

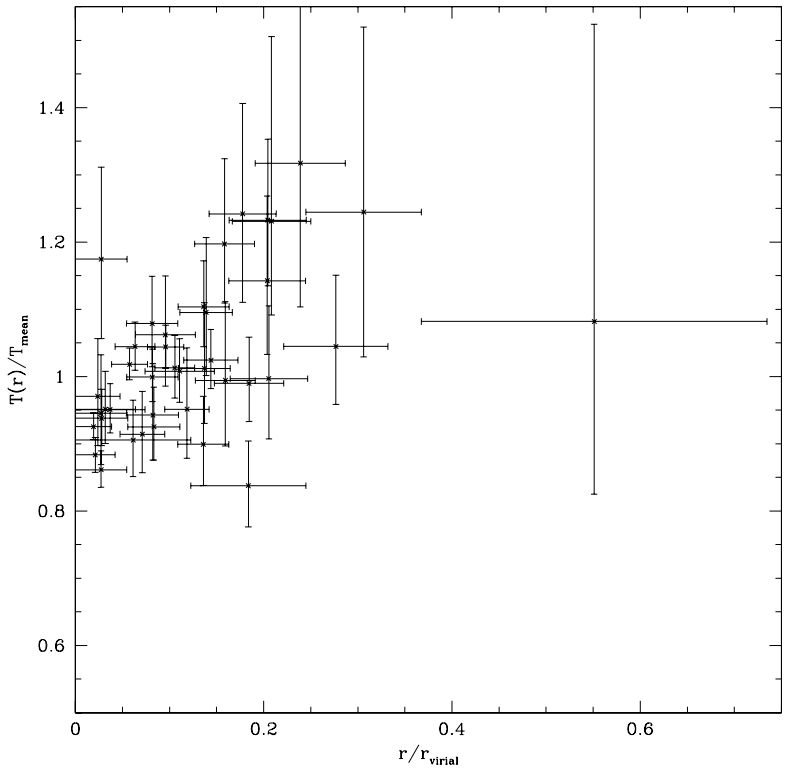

Figure 4: (*a*) Normalized temperature profiles for all 11 clusters in the sample versus radius in units of the virial radius.

a PI energy bin by PI energy bin basis. Once an energy has been assigned to each event in the deconvolved plane, the event list can be analyzed via standard spectral-fitting procedures.

Both methods have their advantages and disadvantages. Whereas method WB employs only a spatially-invariant PSF, method M uses a PSF that varies with position. On the other hand, method M is reliant on *ROSAT* data to determine the emissivity profile, while method WB is not. It is not clear if the emissivity profile derived from the 0.2–2.0 keV *ROSAT* band is appropriate for use over the *ASCA* bandpass. The only way to determine which of these disadvantages are leading to incorrect results is to create simulated data with a known temperature and surface brightness profile and convolve it with the response of the instrument, and then see if the PSF-correction technique can recover the input temperature and surface brightness profiles. White & Buote (1999) have tested their code on simulated cluster data with a giant cooling flow model, a medium cooling flow model, an isothermal profile, and a profile that decreases by a factor of two from the center out to $20'$, as well as data of varying signal-to-noise ratios. In all cases, the original temperature and surface brightness profiles are recovered. Conversely, method M has not been as extensively tested on a variety of simulated temperature distributions and signal-to-noise ratios.

As a final note, it should be noted that Markevitch et al. (1998) used a cooling flow model to fit the innermost bin of cooling flow clusters, whereas White (1999) used a single component thermal model. This will naturally lead to a lower value for White (1999) for the innermost bin (typically $\sim 5\%$ of the virial radius). However, White (1999) claims that correcting for the cooling gas leads to an ambient core temperature within the innermost bin consistent with the outer regions of the cluster. Again, this is inconsistent with the results of Markevitch et al. (1998) who find a value for the ambient core temperature greater than the rest of the cluster.

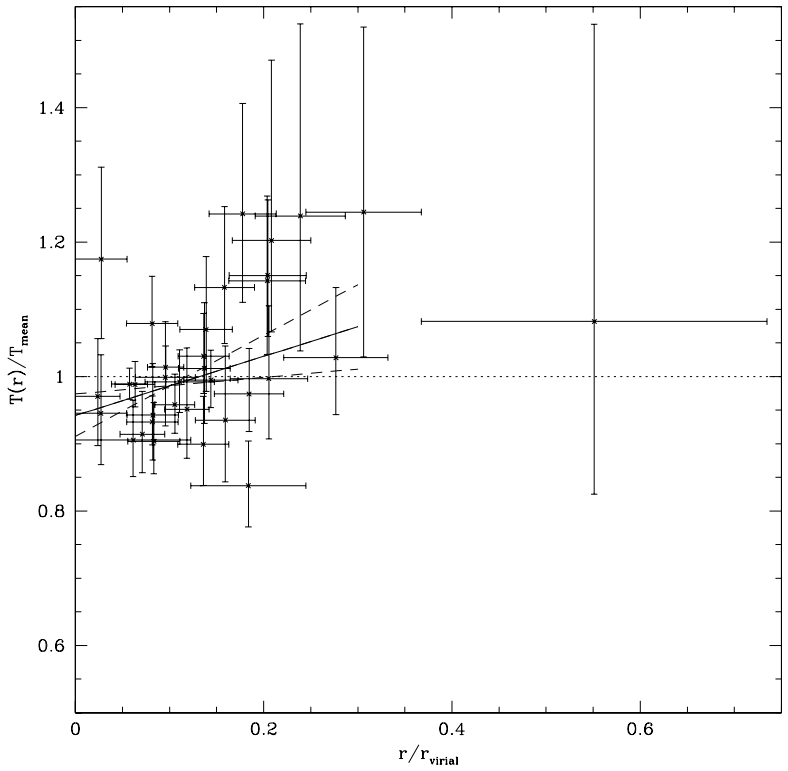

Figure 4: (*b*) Normalized temperature profiles after compensating for the effect of cooling flows (see text). Error bars represent the 1 σ errors. The solid line is the best-fit linear function, with the dotted lines representing the 90% confidence levels of the slope.

4.2 Temperature Profiles Determined With ROSAT

Although the limited bandpass of the *ROSAT* PSPC (0.2-2.4 keV) precludes tight constraints to be put on the temperatures of hot clusters, large (factor of two) temperature changes should be detectable with large enough signal-to-noise ratios. Unfortunately, most clusters observed with *ROSAT* did not have good enough statistics to accomplish this on an individual basis. To circumvent this problem, Irwin et al. (1999) averaged together the radial color profiles (ratio of counts in various bands covering the *ROSAT* PSPC bandpass) of 26 clusters observed with the PSPC. If large-scale deviations from isothermality were common in clusters, such a feature lost in the noise for an individual cluster would become apparent when the clusters were added together. Although a drop in temperature was found in the center of cooling flow clusters (indicating that the method could indeed detect changes in temperatures even for hot clusters), the temperature profiles were flat outside of the cooling region out to 35% of the virial radius. It was found that a 20% temperature drop within 35% of the virial radius was ruled out at the 99% confidence level. This is in agreement with the *BeppoSAX* data presented here, where a decline in temperature of 14% out to 30% of the virial radius is ruled out at the 99% confidence level.

4.3 Temperature Profiles Determined With BeppoSAX

Several of the clusters in our sample have been analyzed by other authors: A2199 (Kaastra et al. 1998), A2029 (Molendi & De Grandi 1999), A2319 (Molendi et al. 1999), and A3266 (De Grandi & Molendi 1999). The profile of A2199 is fully consistent with ours. For the other three clusters, somewhat different steps were taken in the data reduction process than what we did.

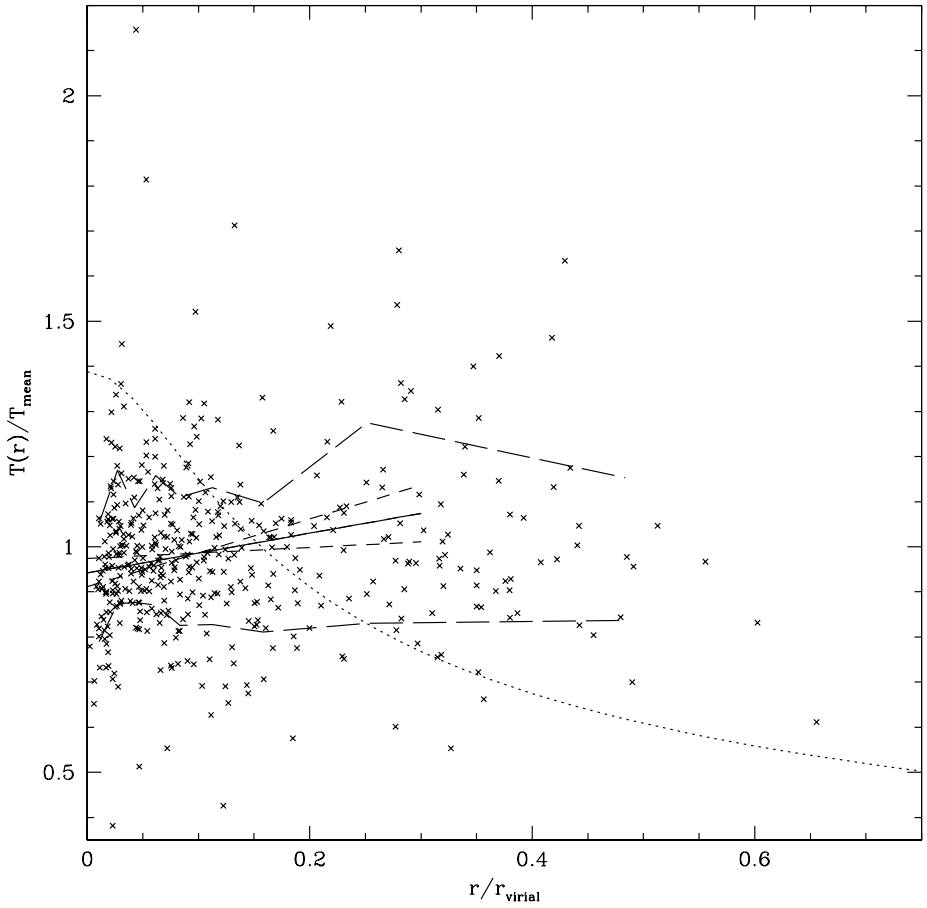

Figure 5: Summary of cluster temperature profiles to date. The normalized temperature profiles of 98 clusters observed by White (1999) as a function of the virial radius are shown as crosses. The long dotted lines enclose the middle 68% of the data points. Also shown is the Markevitch et al. (1998) result (dotted line). The solid line with the accompanying dashed lines represents the composite temperature profile presented in this paper along with the 90% errors in the slope of the best-fit line.

Whereas we excluded data below 3.0 keV, other authors have included data down to 2.0 keV. In addition, they have frozen the redshift whereas we have let it be a free parameter. We have re-analyzed the *BeppoSAX* data for these three clusters, this time including data down to 2.0 keV and freezing the redshift. Although inclusion of channels below 3.0 keV lowered the derived temperatures somewhat (see § 3.1), it did not change the overall shape of the profiles.

Our new profile of A2319 was consistent with that of Molendi et al. (1999). The profiles of A2029 and A3266 differed somewhat from Molendi & De Grandi (1999) and De Grandi & Molendi (1999). However, the differences occurred only in the $2'-4'$ bins, with our 1σ error bars overlapping their 1σ error bars for the other three spatial bins. For both A2029 and A3266 our $2'-4'$ temperature was $\sim$1.5 keV lower than those obtained by Molendi & De Grandi (1999) and De Grandi & Molendi (1999), and the difference was significant at the 3.3σ and 1.9σ confidence levels for A2029 and A3266, respectively. The cause of this discrepancy may be the choice of the assumed surface brightness profile, especially for the case of A2029, which possesses a large cooling flow. As mentioned in § 7, we have used the double-beta model profile obtained by Mohr et al. (1999) from *ROSAT* PSPC data. It is not stated where the other authors obtained their assumed surface brightness profiles. However, the agreement between the other three spatial bins (especially the first and fourth spatial bins) is encouraging, indicating a flat temperature profile out to $9'$ for A2029 and A2319, and a modestly decreasing profile for A3266. It should be noted

that Molendi & De Grandi (1999) and De Grandi & Molendi (1999) find significant temperature drops in A2029 and A3266, respectively, at very large radii, where we have truncated our profiles because of the presence of the strongback, and the increasing asymmetry of the PSF at larger radii.

5 A Summary of Cluster Temperature Profiles

Given the effort put forth in determining temperature profiles for a large sample of clusters in recent years it is worthwhile to summarize the major contributions to this subject: Markevitch et al. (1998; and references within) and White (1999) with *ASCA* data, Irwin et al. (1999) with *ROSAT* PSPC data, and this current study with *BeppoSAX* data. The combined results are shown in Figure 5. The 98 temperature profiles of White (1999) (shown as crosses) have been normalized to the global temperature for each individual cluster and scaled in units of the virial radius. The long dashed lines enclose the middle 68% of the data points. The error bars are typically rather large for each data point, and have been excluded for clarity. The temperature profile derived by Markevitch et al. (1998) is shown as a dotted line, and represents a fit with polytropic index of $\gamma = 1.24$. The results presented in this paper is shown as a solid line. The *ROSAT* PSPC result is not shown but is very similar to best-fit line derived here, only somewhat less constrained.

The results of White (1999), Irwin et al. (1999), and this study all point to the same general conclusion: outside of the cooling region but inside 30% of the virial radius there appears to be no decline in the temperature profile. White (1999) extends this result out to 45% of the virial radius, although it should be noted that large drops in the temperature have been found in A2029 and A3266 with *BeppoSAX* data (Molendi & De Grandi 1999; De Grandi & Molendi 1999) in this region. Outside of 45% of the virial radius White (1999) finds evidence for a decline in temperature although the statistics are sparse in this region. This drop is not surprising though since nearly all cluster simulations show a decline in temperature at large radii.

Acknowledgments

JAI thanks R. Dupke for many useful comments and conversations. We thank D. White for kindly providing us with his *ASCA* temperature profiles, and also the anonymous referee for many insightful comments and suggestions to improve the paper. This research has made use of data obtained through the High Energy Astrophysics Science Archive Research Center Online Service, provided by the NASA/Goddard Space Flight Center, and also the *BeppoSAX* Science Data Center. This work has been supported by *Chandra* Fellowship grant PF9-10009, awarded through the *Chandra* Science Center. The *Chandra* Science Center is operated by the Smithsonian Astrophysical Observatory for NASA under contract NAS8-39073.

References

1. Boella, G., Chiappetti, L., Conti, G., Cusumano, G., Del Sordo, S., La Rosa, G., Maccarone, M. C., Mineo, T., Molendi, S., Re, S., Sacco, B., & Tripiciano, M. 1997, A&A, 122, 327
2. Briel, U. G., & Henry, J. P. 1996, ApJ, 472, 131
3. Briel, U. G., & Henry, J. P. 1994, Nature, 372, 439
4. D'Acri, F., De Grandi, S., & Molendi, S. 1998, in The Active X-ray Sky: Results from *BeppoSAX* and RXTE, ed. L. Scarsi, H. Bradt, P. Giommi, and F. Fiore (Amsterdam: Elsevier), 581
5. De Grandi, S., & Molendi, S. 1999, astro-ph/9910413

6. Dupke, R. A., & White, R. E., III. 1999, astro-ph/9902112
7. Ettori, S., & Fabian A. C. 1999, MNRAS, 305, 834
8. Frenk, C. S., et al. 1999, ApJ, 525, 554
9. Fujita, Y., Koyama, K., Tsuru, T., & Matsumoto, H. 1996, PASJ, 48, 191
10. Henry, J. P., & Briel, U. G. 1996, ApJ, 472, 137
11. Ikebe, Y. 1995, Ph.D. thesis, Tokyo Univ.
12. Irwin, J. A., Bregman, J. N., & Evrard, A. E. 1999, ApJ, 519, 518
13. Irwin, J. A., & Sarazin, C. L. 1995, ApJ, 455, 497
14. Kaastra, J. S., Bleeker, J. A. M., & Mewe, R. 1998, in The Active X-ray Sky: Results from *BeppoSAX* and RXTE, ed. L. Scarsi, H. Bradt, P. Giommi, and F. Fiore (Amsterdam: Elsevier), 567
15. Kikuchi, K., Furusho, T., Ezawa, H., Yamasaki, N., Ohashi, T., Fukazawa, Y., & Ikebe, Y. 1999, astro-ph/9903431
16. Kneer, R., Böhringer, H., Neumann, D., & Krautter, J. 1996, in Röntgenstrahlung From the Universe, ed. H. U. Zimmermann, J. Trümper, & H. Yorke (Garching: MPE), 593
17. Markevitch, M. 1996, ApJ, 465, L1
18. Markevitch, M., Mushotzky, R., Inoue, H., Yamashita K., Furuzawa, A., & Tawara, Y. 1996, ApJ, 456, 437
19. Markevitch, M., Forman, W. R., Sarazin, C. L., & Vikhlinin, A. 1998, ApJ, 503, 77
20. Markevitch, M., & Vikhlinin, A. 1997, ApJ, 474, 84
21. Markevitch, M., Vikhlinin, A., Forman, W. R., & Sarazin, C. L. 1999, astro-ph/9904382
22. Mohr, J. J., Mathiesen, B., & Evrard, A. E. 1999, ApJ, 517, 627
23. Molendi, S. 1998, *BeppoSAX* Technical Report, ftp://www.sdc.asi.it/pub/sax/doc/reports/arf-extended_sources.ps.gz
24. Molendi, S., & De Grandi, S. 1999, astro-ph/9910284
25. Molendi, S., De Grandi, S., Fusco-Femiano, R., Colafrancesco, S., Fiore, F., Nesci, R., & Tamburelli, F. 1999, astro-ph/9909228
26. Mushotzky, R., Loewenstein, M., Arnaud, K., & Fukazawa, T. 1995, in AIP Conf. Proc. 336, Dark Matter, ed. S. S. Holdt and C. L. Bennett (New York: AIP), 231
27. Ohashi, T., Honda, H., Ezawa, H., & Kikuchi, K. 1997, in X-ray Imaging and Spectroscopy of Cosmic Hot Plasmas, ed. F. Makino & K. Mitsuda (Tokyo:Universal Academy), 49
28. Peres, C. B., Fabian, A. C., Edge, A. C., Allen, S. W., Johnstone, R. M., & White, D. A. 1998, MNRAS, 298, 416
29. Pislar, V., Durret, F., Gerbal, D., Lima Neto, G. B., & Slezak, E. 1997, A&A, 322, 53
30. Sarazin, C. L., Wise, M. W., & Markevitch, M. L. 1998, ApJ, 498, 606
31. Takahashi, T., Markevitch, M., Fukazawa, Y., Ikebe, Y., Ishisaki, Y., Kikuchi, K., Makishima, K., & Tawara, Y. 1995, *ASCA* Newsletter, #3 (NASA/GSFC)
32. White, D. A. 1999, astro-ph/9909467
33. White, D. A. & Buote, D. A. 1999, astro-ph/9909457

Constructing the Universe with Clusters of Galaxies, IAP 2000 meeting, Paris (France) July 2000
Florence Durret & Daniel Gerbal eds.

Radial Abundance Profiles of 12 Clusters of Galaxies Observed With *BeppoSAX*


Jimmy A. Irwin and Joel N. Bregman

We have derived azimuthally-averaged radial iron abundance profiles of the X-ray gas contained within 12 clusters of galaxies with redshift $0.03 \leq z \leq 0.2$ observed with *BeppoSAX*. We find evidence for a negative metal abundance gradient in most of the clusters, particularly significant in clusters that possess cooling flows. The composite profile from the 12 clusters resembles that of cluster simulations of Metzler & Evrard (1997). This abundance gradient could be the result of the spatial distribution of gas-losing galaxies within the cluster being more centrally condensed than the primordial hot gas. Both inside and outside the core region, we find a higher abundance in cooling flow clusters than in non-cooling flow clusters. Outside of the cooling region this difference cannot be the result of more efficient sputtering of metals into the gaseous phase in cooling flow clusters, but might be the result of the mixing of low metallicity gas from the outer regions of the cluster during a merger.

6 Introduction

The presence of metals in the hot gas contained within clusters of galaxies provides important clues as to how metals are deposited into the intracluster medium (ICM) from the constituent galaxies of the cluster. The two most likely mechanisms for injecting metals into the ICM are through ram pressure stripping of the gas from galaxies by the ICM (e.g., Gunn & Gott 1972; Gaetz, Salpeter, & Shaviv 1987) and galactic winds (e.g., Ostriker & Yahil 1973; Metzler & Evrard 1994). Recent work has suggested that negative radial abundance gradients are a common feature in clusters. Analysis of *ASCA* data have indicated that in some clusters the metal abundance declines from ∼40%–60% of solar in the center to ∼20% of solar at a distance of 0.5–1 Mpc (Ikebe et al. 1997; Ezawa et al. 1997; Sarazin, Wise, & Markevitch 1998; Finoguenov, David, & Ponman 1999; Dupke & White 2000a,b)

Most of the above studies, however, dealt with groups or cooler clusters. The large, energy-dependent Point Spread Function (PSF) of *ASCA* preferentially scatters hard photons, making spatially-resolved spectroscopy problematic for hot clusters. Whereas the problem is less severe for cooler (< 5 keV) clusters, substantial errors in the radial temperature and abundance profiles can occur if the PSF is not dealt with properly (see Takahashi et al. 1995). As such, little observational work has been done on the radial abundance profiles of hotter clusters. There has also been correspondingly little theoretical work performed on the predicted abundance profiles of clusters from hydrodynamical simulations. White (1999) has derived PSF-corrected abundance profiles for a large sample of clusters observed with *ASCA*, but the deconvolution technique used to correct for the PSF unfortunately led to rather large uncertainties in the derived abundance profiles. As a result, only weak constraints could be placed on the presence

of abundance gradients from these data.

BeppoSAX is better-suited to perform spatially-resolved spectroscopy on hot clusters. The PSF of *BeppoSAX* is one-half that of the *ASCA* GIS, and more importantly, is only weakly dependent on energy. The abundance profiles of five higher temperature clusters have already been derived from *BeppoSAX*, finding at least marginal evidence for abundance gradients in A2029, A2256, A3266, and PKS0745-191, with no evidence for a gradient in A2319 (Molendi & De Grandi 1999; Molendi, De Grandi, & Fusco-Femiano 2000; De Grandi & Molendi 1999a,b; Molendi et al. 1999). In this *Paper*, we increase this sample size by analyzing *BeppoSAX* archival data for 12 clusters of galaxies, and derive radial abundance profiles for each cluster, nine of which have temperatures greater than 5 keV. Throughout this paper, we assume $H_0 = 50$ km s^{-1} Mpc^{-1} and $q_0 = 0.5$.

7 Sample and Data Reduction

From the *BeppoSAX* Science Data Center (SDC) archive (available at http://www.sdc.asi.it/sax_main.html) we have obtained data for 12 clusters of galaxies. Within this sample, eight of them possess cooling flows (A85, A496, A1795, A2029, A2142, A2199, A3562, and 2A0335+096) and four do not (A2163, A2256, A2319, and A3266). We define a cluster as having a cooling flow if the cooling rate is greater than 20 $M_\odot$ yr^{-1}; see Peres et al. 1998 and White, Jones, & Forman 1997. All of the clusters are at low redshift ($0.03 \leq z \leq 0.09$) except for A2163, which has a redshift of $z = 0.203$. We analyze data taken with the Medium Energy Concentrator Spectrometer (MECS) onboard *BeppoSAX*. The MECS (see Boella et al. 1999 for details) is composed of two identical gas scintillation proportional counters (three detectors before 1997 May 9) that are sensitive in the 1.3–10.5 keV energy range. The event files for all 12 clusters were subjected to the standard screening criteria of the *BeppoSAX* SDC.

Since we are interested in deriving the radial abundance profiles for these clusters, it is important to account for scattering owing to the (PSF) of the MECS instrument. Fortunately, the detector + telescope PSF of *BeppoSAX* is nearly independent of energy. This is because the Gaussian PSF of the MECS detector improves with increasing energy, while the PSF of the grazing incidence Mirror Unit degrades with increasing energy (D'Acri, De Grandi, & Molendi 1998), leading to a partial cancellation when these two effects are combined.

To correct for the PSF we have used the routine *effarea*, available as part of the SAXDAS 2.0 suite of *BeppoSAX* data reduction programs. The program *effarea* convolves the surface brightness profile of the cluster (which has been determined using *ROSAT* PSPC data; see Mohr, Mathiesen, & Evrard 1999 and Ettori & Fabian 1999) with the PSF of the MECS to determine the amount of contamination in the spatial region in question at each energy from other regions of the cluster. Thus, an energy-dependent correction vector is formed. When this correction vector is multiplied by the observed spectrum, the PSF-corrected energy spectrum is obtained for the region. In practice, this information is incorporated into the auxiliary response file (the *.arf* file), which is subsequently used in the spectral fitting. This task also corrects for vignetting. A more complete description of the task is given in Molendi (1998) and D'Acri et al. (1998). This correction does not appear to affect the spectrum greatly; D'Acri et al. (1998) and Kaastra, Bleeker, & Mewe (1998) found only small changes between the uncorrected and corrected temperature profiles for Virgo and A2199, respectively. In addition, D'Acri et al. (1998) found that the correction vectors amounted to 5% or less for energies above 3 keV outside of the innermost bin (the innermost bin loses some flux via scattering but gains very little from photons scattered in from greater off-axis radii). Our inner three spatial bins are identical in angular extent to the bins of D'Acri et al. (1998), so we assume that our correction vectors are as small as theirs. In addition, we find only a small difference between our corrected and uncorrected abundance profiles for our sample.

We extracted spectra in four annular regions for each cluster, with inner and outer radii of $0' - 2'$, $2' - 4'$, $4' - 6'$, and $6' - 9'$. At $9'$ the telescope entrance window support structure (the strongback) strongly absorbs X-rays, making spectroscopy difficult in this area of the detector. In addition, for off-axis angles greater than $10'$, the departure of the PSF from radial symmetry becomes noticeable (Boella et al. 1997). With this in mind, we ended the radial profiles at $9'$. At this radius, the profiles extended to 17%–33% of the virial radius, where $r_{virial} = 3.9\ (T/10\ \mathrm{keV})^{1/2}$ Mpc (see Evrard, Metzler, & Navarro 1996), for all clusters except A2163, for which the profile extended to 55% of r_{virial}. We also extracted one global spectrum $(0' - 9')$ and also two spectra covering the two regions $0 - 0.075 r_{virial}$ and $0.075 - 0.173 r_{virial}$. Background was obtained from the deep blank sky data provided by the SDC. We used the same region filter to extract the background as we did the data, so that both background and data were affected by the detector response in the same manner. The energy channels were regrouped to contain at least 25 counts.

For each cluster, XSPEC Version 11.0 was used to fit the spectrum. The MECS2 and MECS3 (and MECS1 when available) data were fit separately, but with the same temperature, metallicity, and normalization. We assumed a MEKAL model with an absorption component fixed at the Galactic value, allowing the temperature and metallicity to vary. For the iron-to-hydrogen ratio we use a value of 4.68×10^{-5} (Anders & Grevesse 1989) since this is the value assumed for most previous abundance determinations, although it should be noted that more recent determinations of the Fe/H ratio point to a value of 3.24×10^{-5} (Ishimaru & Arimoto 1997). Because of a systematic shift of 45–50 eV at 6.6 keV in the MECS channel–to–energy conversion, we have also allowed the redshift to vary (F. Fiore, private communication). This systematic shift was evident in our sample; when the redshift was allowed to vary, the measured redshift was less than the optically-determined redshift in all 12 clusters, and inconsistent with the optically-determined redshift at the 90% confidence level for eight of them. A modest decrease in the reduced χ^2 also occurred for most of the clusters when the redshift was allowed to vary. However, freeing the redshift did not affect the values obtained for the temperature and metallicity by more than 5% (and in most instances much less), so the results do not depend significantly on this shift. We also fit only the 3.0–10.5 keV part of the spectrum because of excess flux found below 3.0 keV that might be the result of uncertainties in the calibration of the MECS instruments; see Irwin & Bregman (2000) for a more complete description. All quoted errors are 90% confidence levels for one interesting parameter ($\Delta\chi^2 = 2.71$) unless otherwise noted. Below we present the results from the abundance analysis. The results of the temperature analysis are given in Irwin & Bregman (2000). One additional cluster (A3562) not analyzed in Irwin & Bregman (2000) is presented here.

8 Abundance of the Hot Gas

8.1 Global Abundances

For hot clusters it is the Fe-Kα line that primarily determines the metal abundance measurement. The fits to the global spectra were adequate, with $\chi^2_\nu < 1.20$ in all cases. For the eight clusters harboring cooling flows, the weighted average emission-weighted global abundance was 0.37 ± 0.04 (the error is given by the weighted standard deviation for the subsample). The four clusters lacking cooling flows had an average emission-weighted global abundance of 0.27 ± 0.02. The ratio of cooling flow to non-cooling flow global abundance is 1.4 ± 0.2, in good agreement with the value of 1.6 obtained by Allen & Fabian (1998) with a sample of 30 clusters observed with *ASCA* when they used a single component thermal model.

8.2 Radial Abundance Profiles

The radial metal abundance profile for each cluster is shown in Figure 6. Four of the clusters have had abundance gradients determined with *ASCA*, and are generally consistent within the errors with the profiles determined here: A496 (Dupke & White 2000b; Finoguenov et al. 1999), A2199 (Finoguenov et al. 1999), A2029 (Sarazin et al. 1998; Finoguenov et al. 1999) and 2A0335+096 (Kikuchi et al. 1999). In addition, analysis of this same *BeppoSAX* data for A2029, A2256, A2319, and A3266 by other authors are in agreement with our results (Molendi & De Grandi 1999; Molendi et al. 1999; De Grandi & Molendi 1999), with the exception of A2256 for which Molendi et al. (2000) found a significantly decreasing profile whereas ours is flat. However, our inability to find an abundance gradient is the result of the short observing time of the data we used; the total observing time of the Molendi et al. (2000) observation was 2.6 times longer than ours, and they were able to place much tighter constraints on the abundance than we were. In both studies, the 1σ error bars overlapped one another.

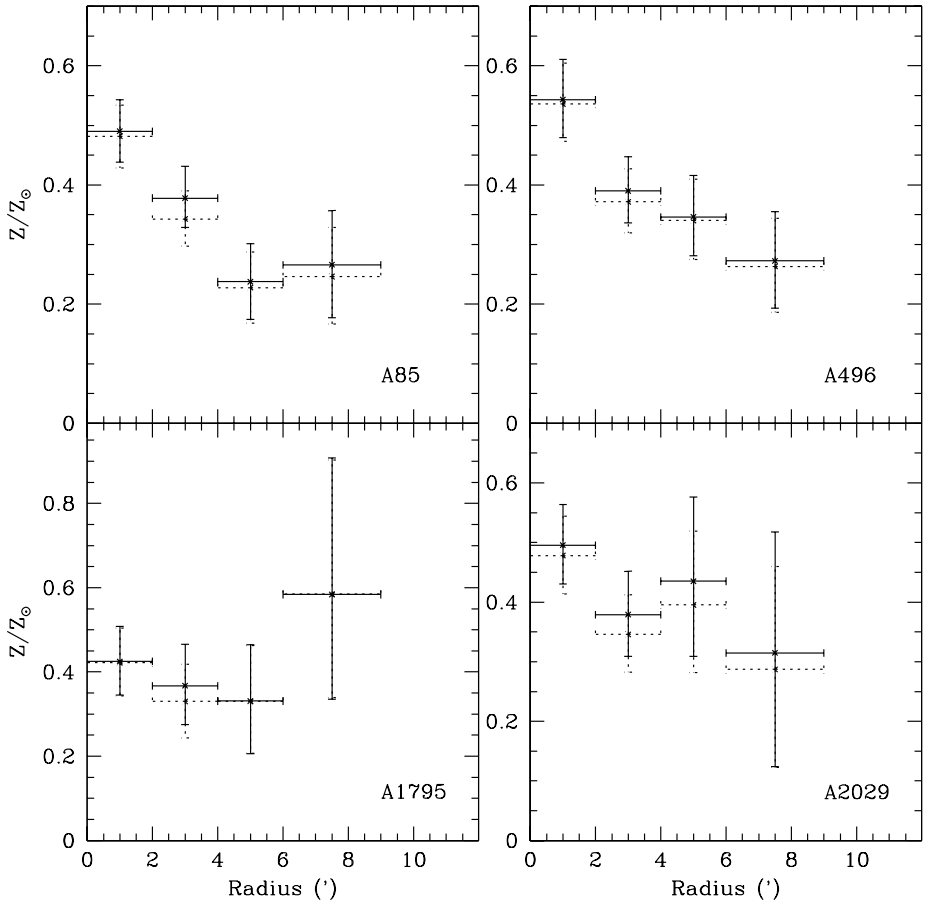

Figure 6: Radial abundance profiles for the 12 clusters in the sample with 90% confidence levels, derived from spectral fitting in the 3.0–10.5 keV energy range. Solid lines represent abundances corrected for the PSF of *BeppoSAX* and the dotted lines are uncorrected for the PSF, except for A2256 where the dotted line represents the *BeppoSAX* profile derived by Molendi et al. (2000) from a longer observation (their error bars have been multiplied by 1.65 to convert 68% confidence levels to 90% confidence levels).

In general, the abundance profiles decline with radius. Such a trend was also found in clusters observed by *ASCA* (Finoguenov et al. 1999; Kikuchi et al. 1999; Dupke & White 2000a), although there are notable exceptions to this trend such as A1060 (Tamura et al. 1996). These previous studies focused primarily on cooler clusters ($kT < 5$ keV). This study confirms the ubiquity of negative abundance gradients in hotter clusters (nine of our 12 clusters have $kT > 5$ keV), as illustrated in Figure 7, where all 12 abundance profiles, normalized to the global abundance for

each cluster, are plotted versus radius in units of the virial radius. A strong negative gradient in the abundance profile is evident out to 25% of the virial radius. However, there are a few points quite discordant with this trend at large radii. The clusters responsible for these discordant points are A1795, A2142, and A2163.

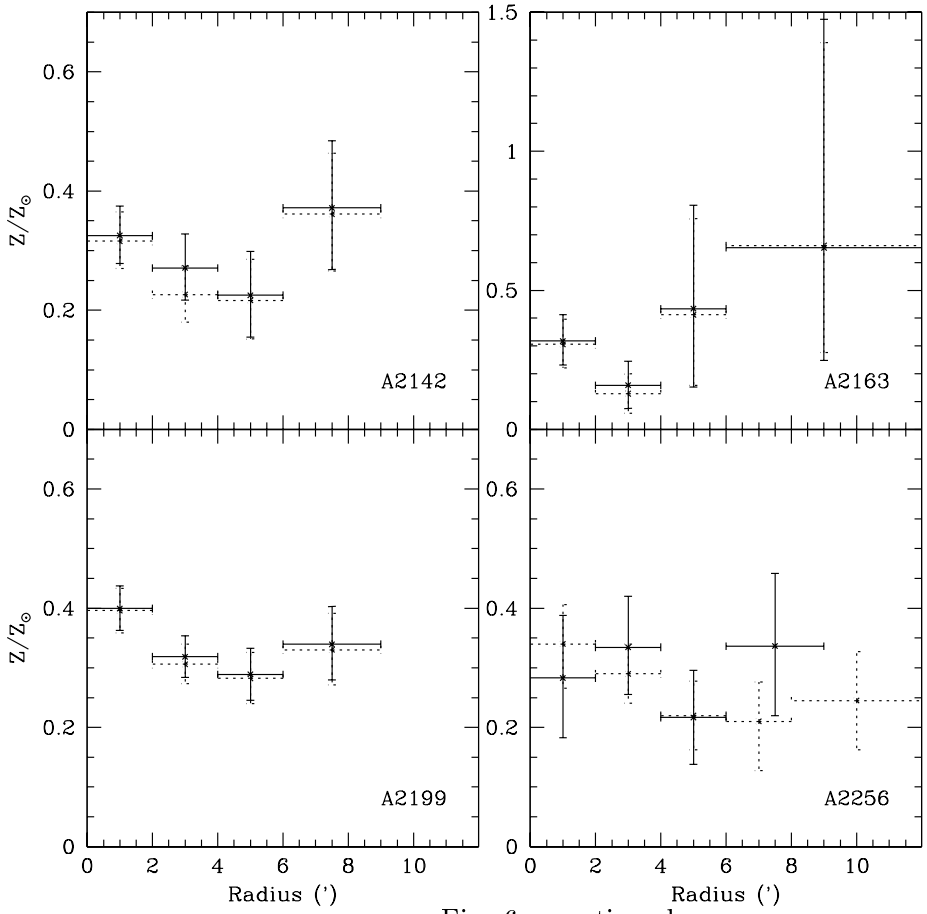

Fig. 6 – continued.

We investigated the possibility that the use of single component temperature models in the central regions of cooling flow clusters has biased the determination of the abundance in these regions. The addition of a cooling flow component did not lead to a significant improvement in the fits, and the cooling rate was only weakly constrained. This is a result of excluding data below 3.0 keV, where the effect of cooling flows on the spectra is most pronounced. When we fixed the cooling rate at values determined by other satellites, the best-fit abundance value was actually slightly *higher* than in the single component case by a few percent, indicating that the central enhancement in the abundance is real.

We have fit a linear model of the form $(Z/Z_{mean}) = a - b(r/r_{virial})$ to the data. While including all values, the fit is not very good, with $\chi^2 = 72.2$ for 47 degrees of freedom, and can be excluded at $> 98\%$ confidence level. Removal of the four discordant data points yielded an excellent fit, with $\chi^2 = 46.1$ for 43 degrees of freedom for values of $a = 1.212$ and $b = 2.705$ (2.149–3.250 at 90% confidence). Although it is not clear why four of the clusters show a $\sim 2\sigma$ departure from the observed trend outside $\sim 25\%$ of the virial radius, the derived slope is nonetheless an accurate representation of the data inside of 25% of the virial radius. Excluding non-cooling flow clusters in addition to the discordant points led to the same best-fit slope.

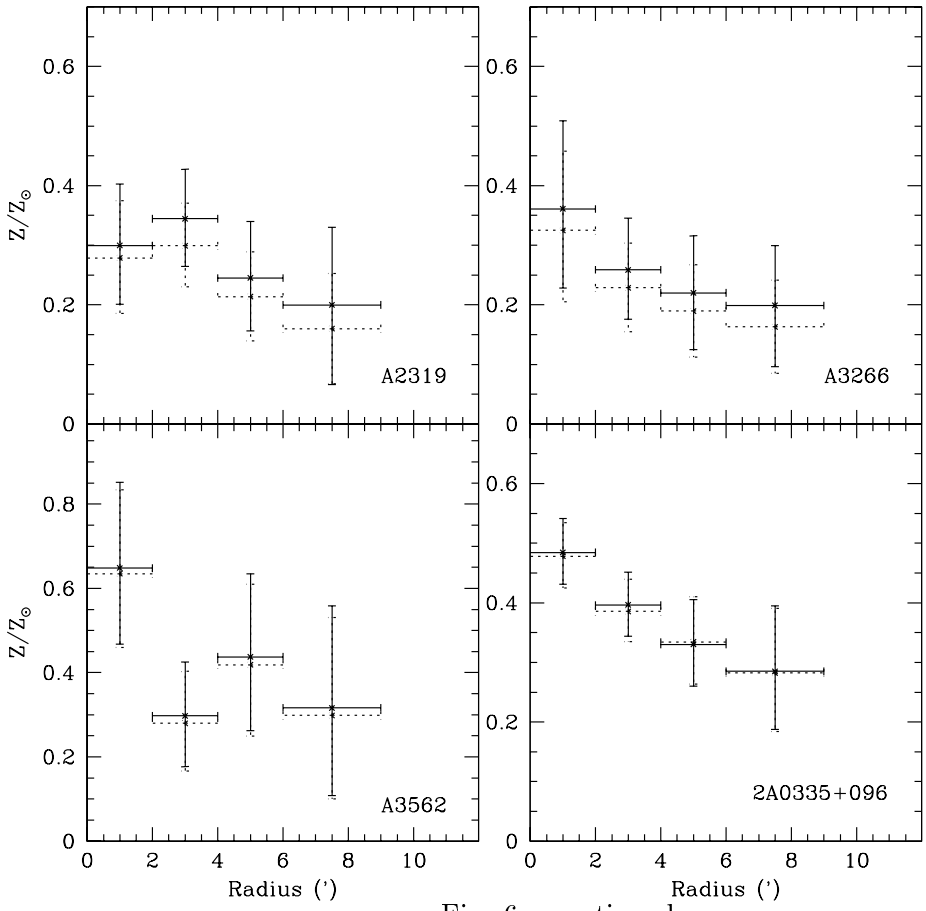

Fig. 6 – continued.

8.3 Comparison To Theoretical Models

Surprisingly little theoretical work has been performed to date to quantify the behavior of abundance gradients in clusters. One such study is that of Metzler & Evrard (1997), who used gas dynamical simulations which included the effects of galactic winds to generate an ensemble of 18 realizations of clusters spanning a wide range of temperatures. Assuming that the iron present in the gas resulted from the ejection of metals from galaxies, a composite iron abundance profile for the 18 realizations was determined. It was found to decrease significantly with increasing radius. This resulted from the spatial distribution of the galaxies being more centrally condensed than the original primordial X-ray gas. Since the ejected gas traces the galaxies, an abundance gradient is created relative to the primordial gas.

The composite iron abundance profile from the 18 three-dimensional realizations of Metzler & Evrard (1997) is shown superposed on the *BeppoSAX* data in Figure 7 as a solid line. The composite profile was normalized assuming an average global abundance of 40% of the solar value. Metzler & Evrard (1997) scaled each cluster in radial units of r_{170} before merging the profiles, where r_{170} is the radius within which the mean density is 170 times the critical density. This is very close to our adopted value of r_{virial}. The normalized abundance profile of Metzler & Evrard (1997) matches the data very well, ranging from a value of 1.3 in the center to about 0.6 at 25% of the virial radius.

We note that recent work by Finoguenov et al. (1999) and Dupke & White (2000b) has shown that significant radial gradients exist in the elemental abundance ratios in clusters. This would argue against the idea that a difference in the spatial distribution between the galaxies and the gas is responsible for the observed abundance gradient if it is assumed that both Type Ia and Type II elements were released into the ICM under the same conditions. The observational

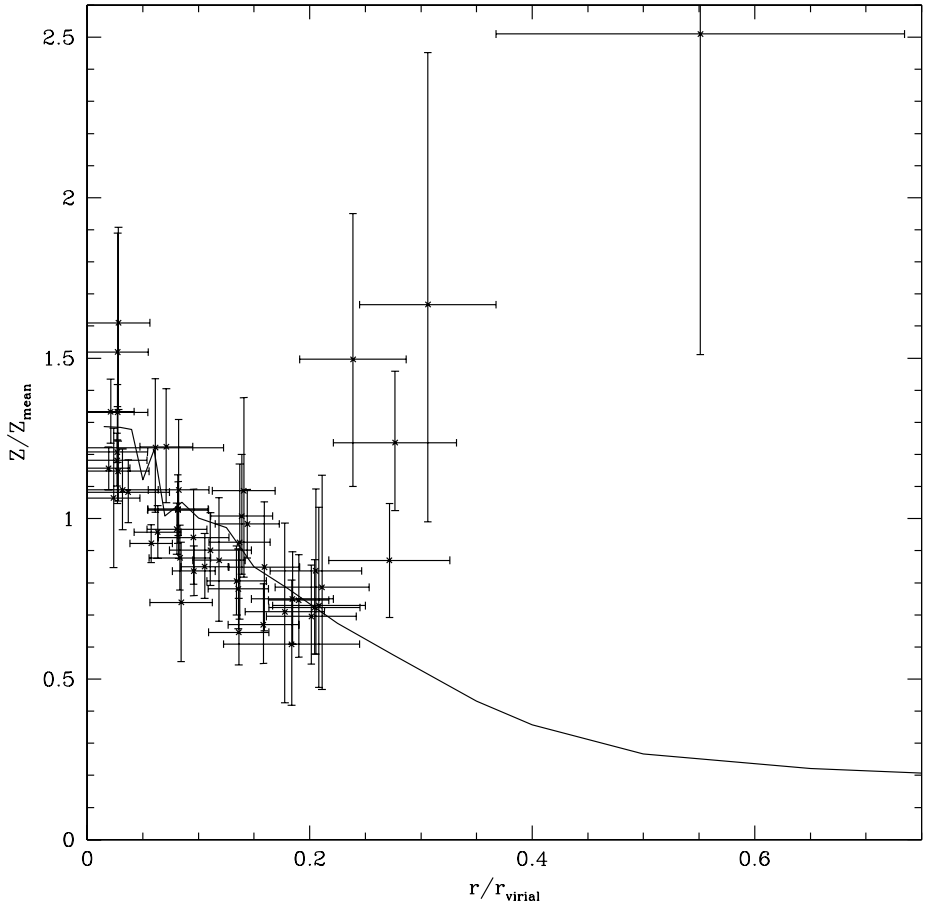

Figure 7: Normalized abundance profiles for all 12 clusters in the sample versus radius in units of the virial radius. Here, the error bars represent the 1σ errors. A significant radial gradient in the abundance is evident. The solid line represents the composite abundance profile of 18 realizations of the cluster simulations of Metzler & Evrard (1997).

evidence implies that Type Ia and Type II elemental contamination is not the same in the inner and outer parts, with Type Ia ejecta being dominant in the center. Dupke & White (2000b) propose that the observed abundance ratios can be explained by a phase of early, vigorous protogalactic wind driven by Type II supernovae that spread metals uniformly throughout the cluster, followed by a phase of less vigorous Type Ia supernovae wind that was suppressed by the central dominant galaxy in the center of the cluster. Thus, the measured iron abundances originate from a combination of Type II supernovae (having no radial gradient) and Type Ia supernovae (having a radial gradient). The gradient we measure is the linear combination of these two effects.

8.4 Cooling Versus Non-cooling Flow Clusters

Inspection of the abundance profiles of the eight cooling flow clusters reveals a radially decreasing trend in all of them. The gradient is quite significant in A85, A496, A2199, A3562, and 2A0335+096, and less significant in A1795, A2029, and A2142. This seems to be a universal trend in cooling flow clusters since all nine cooling flow clusters in the sample of Finoguenov et al. (1999), as well as all three clusters in the samples of Kikuchi et al. (1999) and Dupke & White (2000a) show the same trend, at least marginally. No clear trend exists among the non-cooling flow clusters. The profile of A2256 is flat, although a decline with radius cannot be ruled out owing to the large errors (a decline was seen with a longer *BeppoSAX* observation by Molendi et al. 2000; see Figure 6). A2319, A3266, and A2163 show some evidence for a negative gradient

although the profiles are formally consistent with a flat profile. Results with *ASCA* for clusters with little or no cooling flows are also mixed. Whereas Coma, A401, A1060, and A2670 show a flat abundance profile, A399 has an abundance gradient (Watanabe et al. 1997; Fujita et al. 1996; Tamura et al. 1996; Finoguonov et al. 1999). It is possible that mergers that could be responsible for the disruption of the cooling flow in clusters can also destroy abundance gradients. The degree to which the abundance gradient remains intact may be an indicator of how recent and/or violent the merger was. All four non-cooling flow clusters are merger candidates. Of the five cooling flow clusters with significant gradients, only A85 is a merger candidate. Of the three cooling flow clusters with only weak evidence for an abundance gradients two are recent merger candidates. Oegerle & Hill (1994) conclude that the velocity distribution of galaxies within A1795 suggest that the cluster underwent a merger with a relatively small subcluster such that the cooling flow was not disrupted. Oegerle, Hill, & Fitchett (1995) also find evidence for subclustering from the galaxy velocity distribution in A2142. *ROSAT* PSPC and HRI images of A2142 also suggest that a merger is in process (Henry & Briel 1996). It is possible that mergers have mixed the gas of these two clusters enough to decrease the significance of an abundance gradient without destroying the cooling flow. A2029 does not show evidence for a merger, although the lack of a significant abundance gradient may be the result of poor photon statistics rather than a lack of a gradient. Further studies of A2029 will be needed to confirm this.

As suggested by Fabian et al. (1994) and Allen & Fabian (1998), the presence of abundance gradients in cooling flow clusters provides a reasonable explanation as to why cooling flow clusters have higher emission-weighted metal abundances than their non-cooling flow counterparts. If the cooling gas at the center of clusters has a higher abundance than the outer regions, the strongly peaked X-ray surface brightness distribution characteristic of cooling flow clusters will preferentially weight the global emission-weighted abundance towards the central value, with the low-abundance outer regions contributing relatively little to the global value. Such an effect is not present in non-cooling flow clusters owing to the broader, less-peaked X-ray surface brightness distribution of these clusters. But is this the only reason for the higher measured metallicity in cooling flow clusters, or is there really an abundance difference between cooling flow and non-cooling flow clusters? To test this, we determined abundances in two regions for each cluster, a circle with a radius of $0.075r_{virial}$ and an annulus with inner and outer radii of $0.075r_{virial}$ and $0.173r_{virial}$. The outer radius was set by the need to extend the annulus no further than $9'$ for any cluster, and the inner radius was set to be larger than the cooling radius for any of the cooling flow clusters.

The results are shown in Table 2. Inside of $0.075r_{virial}$ the cooling flow subsample had an average abundance of 0.42 ± 0.06, while the non-cooling flow subsample had an average of 0.33 ± 0.04. In the outer region, the cooling flow subsample had an average abundance of 0.30 ± 0.02, while the non-cooling flow subsample had an average of 0.24 ± 0.03. Thus, there appears to be an abundance gradient in non-cooling flow clusters as well as cooling flow clusters. The presence of abundance gradients in non-cooling flow clusters (especially in hot clusters) would seem to rule out claims that previously observed abundance gradients were artifacts of incorrect spectral modeling due to either the presence of cooling gas at the center of clusters or uncertainties in modeling the Fe-L line complex for cooler clusters.

Although the average abundances of the cooling flow and non-cooling flow clusters are marginally consistent within the errors within the cooling region, the data suggests that there is a discrepancy between the abundance of cooling and non-cooling flow clusters outside of the cooling radius. Of course, any conclusions drawn from a subsample of four clusters should be viewed with caution. A larger sample of clusters will be necessary to confirm if the abundance differences between cooling flow and non-cooling flow clusters are real. This result is in the opposite sense expected if higher metallicity gas from the cooling flow region has been mixed

Table 2:
ABUNDANCES

	kT (keV)[a]	Global	χ^2_ν/d.o.f.	0–0.075 r_{virial}	0.075–0.173 r_{virial}
A85⋆	$6.4^{+0.3}_{-0.2}$	$0.37^{+0.03}_{-0.03}$	1.17/282	$0.45^{+0.04}_{-0.04}$	$0.30^{+0.04}_{-0.05}$
A496⋆	$4.2^{+0.1}_{-0.1}$	$0.41^{+0.03}_{-0.03}$	1.20/259	$0.48^{+0.05}_{-0.04}$	$0.31^{+0.05}_{-0.05}$
A1795⋆	$6.0^{+0.4}_{-0.4}$	$0.39^{+0.05}_{-0.05}$	0.97/211	$0.41^{+0.08}_{-0.07}$	$0.36^{+0.09}_{-0.09}$
A2029⋆	$7.6^{+0.5}_{-0.4}$	$0.43^{+0.05}_{-0.04}$	0.98/141	$0.49^{+0.06}_{-0.06}$	$0.30^{+0.08}_{-0.07}$
A2142⋆	$8.7^{+0.4}_{-0.4}$	$0.30^{+0.03}_{-0.03}$	1.02/292	$0.32^{+0.05}_{-0.05}$	$0.26^{+0.05}_{-0.05}$
A2163	$11.7^{+1.0}_{-0.9}$	$0.26^{+0.06}_{-0.06}$	1.05/440	$0.39^{+0.17}_{-0.14}$	$0.21^{+0.07}_{-0.07}$
A2199⋆	$4.4^{+0.1}_{-0.1}$	$0.35^{+0.02}_{-0.02}$	1.03/419	$0.37^{+0.03}_{-0.03}$	$0.31^{+0.04}_{-0.03}$
A2256	$7.1^{+0.5}_{-0.4}$	$0.28^{+0.04}_{-0.04}$	1.06/238	$0.31^{+0.09}_{-0.08}$	$0.28^{+0.06}_{-0.06}$
A2319	$10.5^{+0.8}_{-0.7}$	$0.28^{+0.05}_{-0.05}$	1.04/273	$0.36^{+0.07}_{-0.07}$	$0.22^{+0.06}_{-0.06}$
A3266	$9.9^{+0.8}_{-0.7}$	$0.24^{+0.05}_{-0.05}$	0.93/265	$0.28^{+0.10}_{-0.10}$	$0.23^{+0.07}_{-0.06}$
A3562⋆	$5.1^{+0.6}_{-0.5}$	$0.40^{+0.08}_{-0.08}$	0.95/165	$0.53^{+0.15}_{-0.14}$	$0.30^{+0.11}_{-0.10}$
2A0335+096⋆	$3.2^{+0.08}_{-0.08}$	$0.41^{+0.03}_{-0.03}$	1.13/257	$0.47^{+0.05}_{-0.05}$	$0.33^{+0.05}_{-0.04}$

⋆cooling flow cluster

[a]Best-fit global temperature of *BeppoSAX* data from Irwin & Bregman (2000), except for A3562 which is presented here for the first time.

in with the lower metallicity gas of the outer regions as the result of a merger in a present-day non-cooling flow cluster. This trend also appeared in a sample of clusters observed by *ASCA*. Fukazawa et al. (1998) analyzed 26 clusters with temperatures of at least 3.0 keV, and found global abundances after having excised the inner cooling regions. The average abundance for the 16 cooling flow clusters was 0.29 ± 0.07, while the average for the ten non-cooling flow clusters was 0.23 ± 0.05. Although at a lower significance than our *BeppoSAX* sample, the trend is in the same direction. Fukazawa et al. (1998) did not claim to extract their spectra in units of the virial radius, which is the unit of distance that allows the most direct comparison of radial properties for clusters of varying sizes and temperatures. This might wash out some of the information on the abundance gradient when the profiles are combined, and lead to a result of lower statistical significance.

Allen & Fabian (1998) present the interesting scenario in which metallicity gradients can be explained (at least in part) by a significant fraction of the metals in clusters residing on grains in cluster cores. Since the lifetime of a grain to sputtering in the hot ICM is inversely proportional to the electron density of the hot gas (e.g., Draine & Salpeter 1979), more metals would be released into the gas phase in the high density cooling flow regions of clusters than in lower density regions, providing the dust grains are ≥ 10 microns. By extending this argument outside the core region, it might be possible to explain the difference in metallicity at large radii between cooling flow and non-cooling flow clusters. If the density of gas outside the core is greater in cooling flow clusters than in non-cooling flow clusters, more metals will be released into the gas phase for the former. A difference in density among cooling and non-cooling flow clusters outside of 200 kpc was observed by White et al. (1997), who deprojected the surface brightness profiles of 207 clusters observed with *Einstein Observatory* and found that the electron densities of clusters with cooling rates greater than 10 $M_\odot$ yr^{-1} were larger than for clusters with cooling rates less than 10 $M_\odot$ yr^{-1} out to a radius of 1 Mpc. For a 7 keV cluster, our $0.075 - 0.173 r_{virial}$ bin corresponds to 240–560 kpc. At a radius of 450 kpc, White et al. (1997) found that the cooling flow clusters had an electron density of $\sim 7 \times 10^{-4}$ cm^{-3}, whereas the non-cooling flow clusters had an electron density of $\sim 3 \times 10^{-4}$ cm^{-3}. For a grain lifetime of 2×10^6 a/n_e yrs (where a is the size of the grain in microns and n_e is the electron density of the hot gas in cm^{-3}), grains with a size of around 2 microns would survive in non-cooling flow clusters for a Hubble

time while being sputtered in cooling flow clusters. While rather large, dust grains of this size are not unreasonable. In addition, this argument assumes that the dust was deposited into the ICM at the time the cluster was created. In reality, dust is deposited into the ICM throughout the history of the cluster, allowing smaller dust grains to survive in low density non-cooling flow clusters while still being sputtered in high density coling flow clusters. This in turn can lead to a higher abundance in the outer regions of cooling flow clusters since more of the grains have been sputtered away owing to the higher electron density.

However, more recent determinations of the density profiles of clusters determined with *ROSAT* PSPC data indicate that the non-cooling flow clusters in our sample do not have a lower electron density in the 0.075–0.173 r_{virial} region than the cooling flow clusters (J. Mohr, private communication). At 10% of the virial radius, the average electron density for the non-cooling flow clusters A2256, A2319, and A3266 was $1.80 \pm 0.20 \times 10^{-3}$ cm^{-3}, while for the cooling flow clusters A85, A496, A1795, A2029, A2142, A2199, and A3562 the average electron was $1.92 \pm 0.46 \times 10^{-3}$ cm^{-3} Thus, it does not appear likely that the difference in abundances outside the cooling radius can be the result of an increased sputtering of grains in cooling flow clusters.

Since non-cooling flow clusters are usually merger candidates, one possible explanation for the difference in abundances between cooling and non-cooling flow clusters is the mixing of gas via mergers from larger ($> 0.175 r_{virial}$) radii rather than from gas interior to this region. If the iron abundance of the gas continues to decline with increasing radius beyond $0.2 r_{virial}$ as the simulations of Metzler & Evrard (1997) imply, the mean metallicity in our 0.075–0.173 r_{virial} bin will be lowered upon mixing with this low metallicity gas during a merger. A2142, a cooling flow cluster that is thought to be undergoing a merger and shows only weak evidence for an abundance gradient, also has the lowest metallicity in the 0.075–0.173 r_{virial} bin among cooling flow clusters in our sample, consistent with the merger-mixing theory. However, A1795, which is also believed to have recently experienced a merger has a high metallicity value in the 0.075–0.173 r_{virial} bin, although the uncertainty is rather large. A larger sample of clusters with abundances determined out to larger radii will be needed to explore this topic further.

9 Conclusions

We have analyzed 12 clusters with the MECS instrument onboard *BeppoSAX* and find evidence for a negative abundance gradient in most of them. This gradient is present in all eight cooling flow clusters, and to a lesser significance in the non-cooling flow clusters. Since $kT > 5$ keV for nine of the 12 clusters, this work extends the ubiquity of abundance gradients to hot clusters. The slope of the abundance gradient is in good agreement with cluster simulations performed by Metzler & Evrard (1997). In our sample cooling flow clusters had a higher metallicity than non-cooling flow clusters both in the inner regions of the cluster and the outer regions out to several hundred kpc; further work with a larger sample will be needed to confirm this result for clusters in general. Outside the cooling region, it seems unlikely that this difference can be explained by the more efficient sputtering of dust grains in cooling flow clusters, since the densities of cooling flow and non-cooling flow clusters are similar in this region. The mixing of low metallicity gas during a merger may be responsible for this difference.

Acknowledgments

We thank the anonymous referee for many useful suggestions and comments. We thank Chris Metzler for making his theoretical abundance profiles available to us. We also thank Joe Mohr for kindly providing us his *ROSAT* PSPC density profiles. JAI thanks Renato Dupke and Gus Evrard for many useful comments and conversations. This research has made use of data ob-

tained through the *BeppoSAX* Science Data Center and the High Energy Astrophysics Science Archive Research Center Online Service, provided by the NASA/Goddard Space Flight Center. This work has been supported by *Chandra* Fellowship grant PF9-10009, awarded through the *Chandra* Science Center. The *Chandra* Science Center is operated by the Smithsonian Astrophysical Observatory for NASA under contract NAS8-39073.

References

1. Allen, S. W., & Fabian, A. C. 1998, MNRAS, 297, L63
2. Anders, E., & Grevesse, N. 1989, Geochimica et Cosmochimica Acta, 53, 197
3. Boella, G., Chiappetti, L., Conti, G., Cusumano, G., Del Sordo, S., La Rosa, G., Maccarone, M. C., Mineo, T., Molendi, S., Re, S., Sacco, B., & Tripiciano, M. 1997, A&A, 122, 327
4. D'Acri, F., De Grandi, S., & Molendi, S. 1998, in The Active X-ray Sky: Results from *BeppoSAX* and RXTE, ed. L. Scarsi, H. Bradt, P. Giommi, and F. Fiore (Amsterdam: Elsevier), 581
5. De Grandi, S., & Molendi, S. 1999a, A&A, 351, L45
6. De Grandi, S., & Molendi, S. 1999b, ApJ, 527, L25
7. Draine, B. T., & Salpeter, E. E. 1979, ApJ, 231, 77
8. Dupke, R. A., & White, R. E., III. 2000a, ApJ, 528, 139
9. Dupke, R. A., & White, R. E., III. 2000b, ApJ, in press
10. Ettori, S., & Fabian A. C. 1999, MNRAS, 305, 834
11. Evrard, A. E., Metzler, C. A., & Navarro, J. F. 1996, ApJ, 469, 494
12. Ezawa, H., Fukazawa, Y., Makishima, K., Ohashi, T., Takahara, F., Xu, H., & Yamasaki, N. Y. 1997, ApJ, 490, L33
13. Fabian, A. C., Crawford, C. S., Edge, A. C., & Mushotzky, R. F. 1994, MNRAS, 267, 779
14. Finoguenov, A., David, L. P., & Ponman T. J. 1999, astro-ph/9908150
15. Fujita, Y., Koyama, K., Tsuru, T., & Matsumoto, H. 1996, PASJ, 48, 191
16. Fukazawa, Y., Makishima, K., Tamura, T., Ezawa, H., Xu, H., Ikebe, Y., Kikuchi, K., & Ohashi, T. 1998, PASJ, 50. 187
17. Gaetz, T. J., Salpeter, E. E., Shaviv, G 1987, ApJ, 316, 530
18. Gunn, J. E., & Gott, J. R. 1972, ApJ, 176, 1
19. Henry, J. P., & Briel, U. G. 1996, ApJ, 472, 137
20. Ikebe, Y., et al. 1997, ApJ, 481, 660
21. Irwin, J. A., & Bregman, J. N. 2000, ApJ, in press
22. Ishimaru, Y., & Arimoto, N. 1997, PASJ, 49, 1
23. Kaastra, J. S., Bleeker, J. A. M., & Mewe, R. 1998, in The Active X-ray Sky: Results from *BeppoSAX* and RXTE, ed. L. Scarsi, H. Bradt, P. Giommi, and F. Fiore (Amsterdam: Elsevier), 567
24. Kikuchi, K., Furusho, T., Ezawa, H., Yamasaki, N., Ohashi, T., Fukazawa, Y., & Ikebe, Y. 1999, astro-ph/9903431
25. Metzler, C. A., & Evrard, A. E. 1997, astro-ph/9710324
26. Metzler, C. A., & Evrard, A. E. 1994, ApJ, 437, 564
27. Mohr, J. J., Mathiesen, B., & Evrard, A. E. 1999, ApJ, 517, 627
28. Molendi, S. 1998, *BeppoSAX* Technical Report, ftp://www.sdc.asi.it/pub/sax/doc/reports/arf-extended_sources.ps.gz
29. Molendi, S., & De Grandi, S. 1999, A&A, 351, L41
30. Molendi, S., De Grandi, S., Fusco-Femiano, R. 2000, astro-ph/0003060
31. Molendi, S., De Grandi, S., Fusco-Femiano, R., Colafrancesco, S., Fiore, F., Nesci, R., & Tamburelli, F. 1999, ApJ, 525, L73

32. Oegerle, W. R., & Hill, J. M. 1994, AJ, 107, 857
33. Oegerle, W. R., Hill, J. M., & Fitchett M. J., AJ, 110, 32
34. Ostriker, A., Yahil, J. P. 1973, ApJ, 185, 787
35. Peres, C. B., Fabian, A. C., Edge, A. C., Allen, S. W., Johnstone, R. M., & White, D. A. 1998, MNRAS, 298, 416
36. Sarazin, C. L., Wise, M. W., & Markevitch, M. L. 1998, ApJ, 498, 606
37. Takahashi, T., Markevitch, M., Fukazawa, Y., Ikebe, Y., Ishisaki, Y., Kikuchi, K., Makishima, K., & Tawara, Y. 1995, *ASCA* Newsletter, #3 (NASA/GSFC)
38. Tamura, T., et al. 1996, PASJ, 48, 671
39. Watanabe, M., Yamashita, K., Kunieda, H., & Tawara, Y. 1997, in X-ray Imaging and Spectroscopy of Cosmic Hot Plasmas, ed. F. Makino & K. Mitsuda (Tokyo:Universal Academy), 131
40. White, D. A. 1999, astro-ph/9909467
41. White, D. A., Jones, C., Forman, W. 1997, MNRAS, 292, 419